C.R.N.

centre de recherches nucléaires de Strasbourg

CRN/PN 86-03

(3, 2)

EXPERIMENTAL ROOT MEAN SQUARE CHARGE RADII, ISOTOPE SHIFTS, GROUND STATE MAGNETIC DIPOLE AND ELECTRIC QUADRUPOLE MOMENTS OF $1 \leq A \leq 239$ NUCLEI

M.S.ANTONY and J.BRITZ

June 1986

Institut National
de Physique Nucléaire
et de Physique
des Particules

Université
Louis Pasteur
de Strasbourg

67037 STRASBOURG CEDEX FRANCE

EXPERIMENTAL ROOT MEAN SQUARE CHARGE RADII, ISOTOPE SHIFTS, GROUND STATE MAGNETIC DIPOLE AND ELECTRIC QUADRUPOLE MOMENTS OF $1 \leq A \leq 239$ NUCLEI

N.S.ANTONY and J.BRITZ

Centre de Recherches Nucléaires et Université Louis Pasteur,

67037 Strasbourg Cedex, France

A compilation of experimental root-mean square charge radii, isotope shifts, ground-state magnetic and electric quadrupole moments of nuclei $1 \leq A \leq 239$ is presented. Shell, sub-subshell closures and changes in nuclear deformations discernible from data are displayed graphically. The nuclear charge distribution, for $1 \leq A \leq 239$ nuclei deduced from Coulomb displacement energies is shown for comparison. References through May 1986 are covered.

CONTENTS

INTRODUCTION

Since the compilation of experimental charge and moment distribution by Boehm (1) and Barret (2), the most recent tables by Heilig (3) deal with changes in mean square nuclear charge radii from optical istope shifts. In the present compilation, root mean square charge radii, isotope shifts, and ground state magnetic and electric quadrupole moments of some of the nuclei $1 \leq A \leq 238$ are presented. Graphical displays of some of the data reveal shell and subshell effects as well as the onset of deformations.

Experimental data of charge distribution in nuclei is of great importance for the understanding of nuclear structure, for they provide valuable informations about the spatial distribution of valence protons and polarisation of the proton core in response to the addition of protons and neutrons. Isotope shifts i.e., the difference in the mean square radii of neighbouring isotopes yield details of the changes in radial moments of the charge distributions between isotopes. Hyperfine splitting allow accurate measurements of the ground state magnetic dipole and electric quadrupole moments of nuclei. Very precise measurements are now capable of deducing the changes in the magnetisation distribution between isotopes.

A parameter of interest for an odd isotope A is the staggering parameter γ defined by

$$\gamma = \frac{2(\langle r^2\rangle_A - \langle r^2\rangle_{A-1})}{(\langle r^2\rangle_{A+1} - \langle r^2\rangle_{A-1})}$$

where $\langle r^2\rangle$ is the mean square charge radius. If there is no staggering $\gamma = 1$ whereas for a charge radius equal to that of the next lowest isotope $\gamma = 0$.

While scattering experiments typically call for milligrams of enriched sample targets, optical methods require much smaller quantities and hence extensible to radioactive isotopes of which only minute quantities can be prepared. High resolution Doppler free laser spectroscopy combined with a sensitive method of detection is currently used for measuring isotope shifts and hyperfine structure of spectral lines (4). A well collimated atomic beam from an on line mass separator is intersected by a light beam of a stablized continuous wave dye laser and the emitted resonance fluorescence photon detected with a photomultiplier. Extension of optical measurements to nuclei far from the valley of stability thus becomes feasible.

The series of stable and unstable isotopes (for example Pb) enables testing of theoretical models in the region of double shell closure where the calculations are physically instructive. For comparison with experimental results one can either adopt a microscopic approach to calculate nuclear densities or use a macrscopic approach as the droplet model (5,6,7). The latter provides a comprehensive description of macroscopic aspects of nuclei such as binding energies and the associated potential energy as a function of the collective coordinates. It also provides a basis for a detailed description of the neutron and proton spatial distribution. While the liquid drop model fails to correctly predict the changes in the nuclear charge radii along isotopic sequences, the droplet model associated with the neutron skin that develops for neutron rich nuclei, seems to be in excellent agreement with measured quantities.

Figures are displayed with comments. Some of the isotopes reveal closed shell and subshell structures from the trend of nuclear charge radii and deformation parameters. Of particular interest is the subshell closure at

N = 64 for the Cd and Sn nuclei. The subshell closure at Z = 64 (Gd) has been well established (8). Sufficient data are available in the rare-earth region to study the influence of this semi magic proton number 64. Deformation effects in the middle of the shell between N = 82 and 126 are reached in a smooth manner. However, a sharp transition takes place for the Gd nuclei between N = 88 and 90 as shown in the ratio E*(2)/E*(1) compared with neighbouring even nuclei as shown below (9) :

Element	Z	N	E*(2)/E*(1)
Ce	58	88	2.585
		90	2.932
Nd	60	88	2.493
		90	2.932
Sm	62	88	2.219
		90	3.009
Gd	64	88	1.788
		90	3.015
Dy	66	88	1.975
		90	2.933
Er	68	88	2.314
		90	2.744

The sharpest rise in the E*(2)/E*(1) ratios for N = 88 to 90 occurs for Gd. A trend in the charge radii differences as well as in deformation effects of the Gd isotope chain should therefore reveal a drastic change when passing from N = 88 to 90, as evidenced from fig.XXIV. The variation of mean square charges for Mo isotopes shows shell closure at N=50 and a subshell closure at N = 56 (Fig.XI), and this result is substantiated from the E*(2)/E*(1) ratios of fig.XII.

The influence of shell structure is clearly visible as an abrupt change in the slope at neutron shell closures. Such a behaviour is interpreted as the superposition of a smoothly varying part, describing nuclear charge radii $\langle r_0 \rangle^2$ with a constant spherical shape and a charge radii $\langle r^2 \rangle$ due to deformation according to

$$\langle r^2 \rangle = \langle r_0 \rangle^2 \left(1 + \frac{5}{4\pi} \langle \beta^2 \rangle\right)$$

where $\langle \beta^2 \rangle$ is the mean square quadrupole deformation parameter.

Experimental root mean square charge radii presented in fig.XXXI include those of $\pi^{\pm}$, K° and K^- as follows :

$\pi^{\pm}$: 0.64 (2)fm (weighted average of ref.10 and 11)

K^- : 0.53 (5)fm (Ref.12)

K° : 0.23 (5)fm (Ref.13)

It is observed that the straight lines joining (a) the elements He-U (b)p,$\pi^{\pm}$ as well as (c)n, and K° are equidistant and parallel. Values of $\langle r^2 \rangle^{1/2}$ plotted in fig.XXXII as a function of quark number reveal that

(a) the line joining charge particles passes through zero quark number.

(b) the line joining neutral particles also passes through zero quark number.

The extrapolated value of the quark core in nucleons(quark number = 1) is = 0.3 fm.to 0.5 fm. Yin He et al (14) predict the rms radius of quarks in nucleons ranging from 0.3 to 0.5 fm.

The purpose of this compilation is to underline the role of optical spectroscopy in the study of nuclear structure. The promising technology of pulsed laser generating ultraviolet laser radiation will be in future a versatile tool for Doppler-free laser spectroscopy. It is hoped that the tables and figures in this work have put together recent data dispersed in literature.

We are grateful to Raymond Seltz, Director of the Centre de Recherches Nucléaires for his encouragement ; Marlène Goetz for typing the manuscript and Béatrice Gress, Charles Lévy and Gérard Hoffmann for the figure preparation.

REFERENCES

1. F.Boehm, *Nuclear charge and Moment Distributions in* ATOMIC DATA AND NUCLEAR DATA TABLES 14, 1(1974).
2. R.C.Barrett and D.F.Jackson, in *Nuclear Sizes and Structures*, (Clarendon Press, Oxford, 1977).
3. K.Heilig, in Hyperfine Interactions 24-26, pp.349 (1985).
4. A.C.Mueller, F.Buchinger, W.Klempt, E.W.Otten, R.Neugart, C.Ekström, J. Heinemeier and the Isolde Collaboration, Nucl.Phys.A403, 234 (1983)
5. W.D.Myers, Nucl.Phys.A204, 465 (1973).
6. W.D.Myers and W.J.Swiatecki, Ann.of Phys.55 , 395 (1969).
7. W.D.Myers and K.-H.Schmidt, Nucl.Phys.A410, 61 (1983).
8. M.S.Antony, Nuovo Cimento 91A, 217 (1986).
9. M.S.Antony, J.Britz and J.B.Bueb, Nuovo Cimento 91A, 283 (1986).
10. E.Dally, D.J.Drickey, J.M.Hauptman, C.F., May, D.H.Stork, J.A.Poirier, C.A.Rey, R.J.Wojslaw, P.F.Shepard, A.J.Lennox, J.C.Tompkins, T.E.Toohig, A.A.Wehmann, I.X.Ioan, T.S.Nigmanov, E.N.Tsyganov, and A.S.Vodopianov, Phys.Rev.Lett.39, 1176 (1977).
11. E.B.Dally, J.M.Hauptman, J.Kubic, D.H.Stork, A.B.Watson, Z.Guzik, T.S.Nigmanov, V.D.Riabtsov, E.N.Tsyganov, A.S.Vodopianov, A.Beretvas, A.Grigorian, J.C.Tompkins, T.E.Toohigs, A.A.Wehmann, J.A.Poirier, C.A. Rey, J.T.Volk, P.D.Rapp and P.F.Shepard, Phys.Rev.Lett.48, 375 (1982).
12. E.B.Dally, J.M.Hauptman, J.Kubic, D.H.Stork, A.B.Watson, Z.Guzik, T.S.Nigomanov, V.D.Riabtsov, E.N.Tsyganov, A.S.Vodopianov, A.Beretvas, A.Grigorian, J.C.Tompkins, T.E.Toohig, A.A.Wehman, J.A.Poirier, C.A.Rey, J.T.Volk, P.D.Rapp, and P.F.Shepard, Phys.Rev.Lett.45, 232 (1980).

13. W.R.Molzon, J.Hoffnagle, J.Roehrig, V.L.Telegdi, B.Winstein,S.H.Aronson, G.J.Bock, D.Hedin, G.B.Thomson and A.Gsponer, Phys.Rev.Lett.41, 1213 (1978).

14. Yin He, Fan Wang, and Chun Wa Wong, Nucl.Phys.A448, 652 (1986).

POLICIES

Sources of information. The basic source of informations are from reviews (74Ja and 77Ba in references for tables and figures). Additional data are taken from original publications.

EXPLANATION OF SYMBOLS IN TABLES AND FIGURES

e	Elastic electron scattering
μ	Muonic-atom charge distribution measurement
DFSS	Doppler-free saturation spectroscopy
LS	Laser spectroscopy
F-PS	Fabry-Perot spectrometer
HFS	Hyperfine X-ray transition
RFS	Resonance fluorescence spectroscopy
OIS	Optical interferometric spectroscopy
BRDOP	Beta-radiation delayed optical pumping
El	Element
Z	Atomic number
N	Number of neutron
A	Mass number
$\langle r^2 \rangle$	Mean square charge radius
RMS	Root mean square
$\langle r^2 \rangle^{1/2}$	Root mean square charge radius
fm	Fermi unit = 10^{-13} cm
$\delta\langle r^2 \rangle^{AA'}$	Changes in mean square charge radii between two isotopes A and A'

$\lambda^{AA'}$	Isotope shifts between two isotopes with mass numbers A and A' observed in the wave number of an atomic spectral line. $\lambda^{AA'}$ is approximately equal to $\delta \langle r^2 \rangle^{AA'}$
γ	Odd-even staggering parameter
μ_N	Magnetic dipole moment
n.m.	Nuclear magneton
$\langle \beta \rangle^2$	Mean Square electric quadrupole deformation parameter
$\langle \beta^2 \rangle^{1/2}$	Root mean square electric quadrupole deformation parameter
$\delta \langle \beta^2 \rangle$	Differences in $\langle \beta^2 \rangle$ between two isotopes
Q_s	Static electric quadrupole moment
E*(2)	Energy of the second excited level
E*(1)	Energy of the first excited level
B(E0)	Monopole transition rates
B(E2)	Reduced E2 transition rates
ρ^2	E0 strength parameter

Element	Z	N	$\langle r^2 \rangle^{1/2}$ (fm)	Method	References
n	0	1	0.3359(36)		74Ja
H	1	0	0.881	e	76Ch
		1	2.095 (6)	e	77Ba
		2	1.70 (5)	e	77Ba
He	2	1	1.976 (15)	e	85Ot
		2	1.671 (14)	e	85Ot
Li	3	3	2.51 (10)	e	72Bu
		4	2.35 (10)	e	72Bu
B	5	5	2.44 (6)	μ	81Ol
		6	2.38 (4)	μ	81Ol
C	6	6	2.4715(160)	μ	82Sc
		7	2.4628(39)	μ	85Bo
		8	2.4962(190)	μ	82Sc
N	7	7	2.540 (20)	e	75Wo
		8	2.580 (26)	e	75Wo
O	8	8	2.718 (21)	e	75Wo
		9	2.710 (15)	e	78Ki
		10	2.789 (27)	e	75Wo
F	9	10	2.898 (10)	μ	78Sc
Ne	10	10	3.020 (20)	e	74Ja
		12	2.969 (21)	e	74Ja
Na	11	12	2.986 (9)	μ	78Sc
Mg	12	12	2.985 (30)	e	74Li
Al	13	14	3.058 (5)	μ	78Sc
Si	14	14	3.129 (3)	μ	78Sc
P	15	16	3.187 (3)	μ	78Sc

Element	Z	N	$\langle r^2 \rangle^{1/2}$ (fm)	Method	References
S	16	16	3.248 (4)	e	83Ry
		18	3.281 (4)	e	83Ry
		20	3.278 (6)	e	83Ry
Cl	17	18	3.388 (15)	e	80Br2
		19	3.384 (15)	e	80Br2
Ar	18	18	3.396 (7)	μ	74Da
		20	3.410 (11)	μ	74En
		22	3.423 (6)	μ	74Da
K	19	20	3.4378(50)	μ	81Wo
		22	3.4549(50)	μ	81Wo
Ca	20	20	3.4813(50)	μ	81Wo
		21	3.480(6)	μ	79Ko
		22	3.5115(50)	μ	81Wo
		23	3.4980(50)	μ	81Wo
		24	3.5214(50)	μ	81Wo
Ca	20	26	3.5024(50)	μ	81Wo
		28	3.4823(50)	μ	81Wo
Sc	21	24	3.5498(50)	μ	81Wo
Ti	22	24	3.6094(50)	μ	81Wo
		25	3.5984(50)	μ	81Wo
		26	3.5956(50)	μ	81Wo
		27	3.5770(50)	μ	81Wo
		28	3.5743(50)	μ	81Wo
V	23	28	3.6033(50)	μ	81Wo

Element	Z	N	$\langle r^2 \rangle^{1/2}$ (fm)	Method	References
Cr	24	26	3.6645(50)	μ	81Wo
		28	3.6452(50)	μ	81Wo
		29	3.6620(50)	μ	81Wo
		30	3.6902(50)	μ	81Wo
Mn	25	30	3.7096(50)	μ	81Wo
Fe	26	28	3.700 (5)	μ	76Sh
		30	3.7412(50)	μ	81Wo
		31	3.759 (5)		76Sh
		32	3.780 (5)	μ	76Sh
Co	27	32	3.793 (5)	μ	76Sh
Ni	28	30	3.781 (5)	μ	76Sh
		32	3.818 (5)	μ	76Sh
		33	3.829 (5)	μ	76Sh
		34	3.847 (5)	μ	76Sh
		36	3.866 (5)	μ	76Sh
Cu	24	34	3.888 (5)	μ	76Sh
		36	3.908 (5)	μ	76Sh
Zn	30	34	3.933 (5)	μ	76Sh
		36	3.954 (5)	μ	76Sh
		38	3.971 (5)	μ	76Sh
		40	3.989 (5)	μ	76Sh
Ge	32	38	4.07 (2)	e	75K1
		40	4.05 (3)	e	75k1
As	33	42	4.104 (4)	μ	77Ba
Kr	36	50	4.188 (12)		79Ge
Sr	38	50	4.227 (7)	μ	77Ba
Y	39	50	4.239 (7)	μ	77Ba

Element	Z	N	$\langle r^2 \rangle^{1/2}$ (fm)	Method	References
Zr	40	50	4.263 (8)		76Ro
		51	4.309 (22)	μ	71Fa
		52	4.300 (22)	e	71Fa
		54	4.332 (22)	e	71Fa
		56	4.396 (22)	e	71Fa
Nb	41	52	4.3175(28)		74En
Mo	42	50	4.317 (4)	μ	80Sc
		52	4.352 (4)	μ	80Sc
		53	4.362 (4)	μ	80Sc
		54	4.383 (4)	μ	80Sc
		55	4.387 (4)	μ	80Sc
		56	4.407 (4)	μ	80Sc
		58	4.443 (4)	μ	80Sc
Rh	45	58	4.510 (44)	μ	74En
Pd	46	64	4.595 (3)	e	76Li
Ag	47	60	4.542 (3)	μ	77Ba
		62	4.563 (3)	μ	77Ba
Cd	48	58	4.566 (3)	DFSS	81We
		60	4.581 (3)	DFSS	81We
		62	4.596 (3)	DFSS	81We
		64	4.611 (3)	DFSS	81We
		66	4.624 (8)	DFSS	81We
		68	4.634 (3)	DFSS	81We
In	49	66	4.619 (15)	μ	74En

Element	Z	N	$\langle r^2 \rangle^{1/2}$ (fm)	Method	References
Sn	50	62	4.586 (5)	e	72Fi
		64	4.602 (5)	e	72Fi
		66	4.623 (5)		80Ca
		67	4.625 (5)	e	72Fi
		68	4.634 (5)	e	72Fi
		69	4.639 (5)	e	72Fi
		70	4.646 (5)	e	72Fi
		72	4.658 (5)	e	72Fi
		74	4.670 (5)	e	72Fi
Sb	51	70	4.676 (5)	μ	74En
Te	52	74	4.774 (6)	μ	74En
I	53	74	4.763 (6)	μ	74En
Cs	55	78	4.800 (7)	μ	74En
Ba	56	78	4.8315(14)	μ	83Ku
		79	4.8223(18)	μ	82Sh
		80	4.8320(11)	μ	83Ku
		81	4.8252(21)	μ	82Sh
		82	4.8354(10)	μ	83Ku
La	57	82	4.861 (8)	μ	74En
Ce	58	82	4.883 (9)	μ	74En
Pr	59	82	4.881 (9)	μ	74En

Element	Z	N	$\langle r^2 \rangle^{1/2}$ (fm)	Method	References
Nd	60	82	4.914 (30)	e	71He
		84	4.970 (35)	e	71He
		86	4.970 (35)	e	71He
		88	5.009 (80)	e	71He
		90	5.048	e	71He
Sm	62	82	4.947 (9)	e	81Mo
		86	5.002 (6)	e	81Mo
		88	5.045 (6)	e	81Mo
		90	5.093 (6)	e	81Mo
Gd	64	90	5.123 (3)	μ	83La
		91	5.127 (3)	μ	83La
		92	5.141 (3)	μ	83La
		93	5.143 (3)	μ	83La
		94	5.518 (3)	μ	83La
		96	5.172 (3)	μ	83La
Au	79	118	5.434 (2)	μ	74En
Hg	80	124	5.490 (14)	μ	74En
Tl	81	122	5.472 (6)	μ	74En
		124	5.484 (6)	μ	74En
Pb	82	122	5.486 (1)	μ	77Ba
		124	5.4839(28)	μ	74En
		125	5.504 (1)	e	77Ba
		126	5.503 (2)		80Ca
Bi	83	126	5.513 (7)	μ	74En
Th	90	142	5.7734	e	74Ja
U	92	146	5.7834	e	74Ja

El	Z	A'	A	$\delta\langle r^2\rangle^{AA'}$ (fm^2)		Method	References
Na	11	25	21	0.22	(8)	LS	78Hu
			22	0.05	(6)	LS	78Hu
			23	0.10	(3)	LS	78Hu
			24	0.08	(5)	LS	78Hu
			25	0		LS	78Hu
			26	0.145	(35)	LS	78Hu
			27	0.22	(5)	LS	78Hu
			28	0.38	(6)	LS	78Hu
			29	0.70	(9)	LS	78Hu
			30	0.86	(12)	LS	78Hu
			31	1.19	(8)	LS	78Hu
K	19	39	38	-0.058	(41)	LS	82To
			39	0		LS	82To
			40	0.0222	(20)	LS	82To
			41	0.117	(6)	LS	82To
			42	0.116	(15)	LS	82To
			43	0.143	(9)	LS	82To
			44	0.148	(11)	LS	82To
			45	0.176	(13)	LS	82To
			46	0.143	(12)	LS	82To
			47	0.126	(13)	LS	82To

El	Z	A^h	A	$\delta\langle r^2\rangle^{AA'}$ (fm^2)		Method	References
Ca	20	40	40	0		LS	82An
			41	-0.012	(7)	LS	82An
			42	0.221	(12)	LS	82An
			43	0.117	(6)	LS	82An
			44	0.293	(12)	LS	82An
			45	0.128	(20)	LS	82An
			46	0.128	(8)	LS	82An
			47	0.007	(10)	LS	82An
			48	0.000	(9)	LS	82An
Ni	28		58	0		F-PS	80St
			60	0.218	(40)	F-PS	80St
			61	0.283	(43)	F-PS	80St
			62	0.388	(53)	F-PS	80St
			64	0.498	(42)	F-PS	80St
Kr	36	86	78	-0.1263	(402)	LS	79Ge
			80	-0.0866	(348)	LS	79Ge
			82	-0.0538	(208)	LS	79Ge
			84	-0.0327	(201)	LS	79Ge
			86	0			79Ge
Rb	37	87	76	0.220	(27)	LS	81Th1
			77	0.2831	(69)	LS	81Th1
			78	0.3060	(23)	LS	81Th1

El	Z	A'	A	$\delta\langle r^2\rangle^{AA'}$ (fm^2)		Method	References
Rb	37	87	78m	0.1912	(26)	LS	81Thl
			79	0.2249	(23)	LS	81Thl
			80	0.2166	(68)	LS	81Thl
			81	0.1698	(22)	LS	81Thl
			81m	0.1398	(2)	LS	81Thl
			82	0.1322	(65)	LS	81Thl
			82m	0.1319	(58)	LS	81Thl
			83	0.0512	(15)	LS	81Thl
			84	0.0078	(32)	LS	81Thl
			84m	0.004	(16)	LS	81Thl
			85	0.0355	(22)	LS	81Thl
			86	0.0271	(31)	LS	81thl
			87	0		LS	81Thl
			88	0.1364	(78)	LS	81Thl
			89	0.3051	(31)	LS	81Thl
			90	0.4289	(80)	LS	81Thl
			90m	0.4149	(31)	LS	81Thl
			91	0.5580	(31)	LS	81Thl
			92	0.6963	(80)	LS	81Thl
			93	0.8130	(32)	LS	81Thl
			94	0.9167	(35)	LS	81Thl
			95	1.0781	(56)	LS	81Thl
			96	1.1637	(74)	LS	81Thl
			97	1.7391	(62)	LS	81Thl
			98	1.821	(15)	LS	81Thl

El	Z	A'	A	$\delta\langle r^2\rangle^{AA'}$ (fm^2)		Method	References
Sr	38	88	84	0.110	(10)	LS	84Be
			86	0.047	(6)	LS	84Be
			87	0.007	(7)	LS	84Be
			88	0		LS	84Be
Mo	42	50	92	0		F-PS	78Au
			94	0.226	(19)	F-PS	78Au
			95	0.287	(19)	F-PS	78Au
			96	0.419	(25)	F-PS	78Au
			97	0.446	(25)	F-PS	78Au
			98	0.569	(28)	F-PS	78Au
			100	0.796	(34)	F-PS	78Au
Ag	47		60	0		OIS	75Fi
			61m	0.022	(3)	OIS	75Fi
			62	0.144	(9)	OIS	75Fi
			63m	0.173(9)		OIS	75Fi
Cd	48	114	106	-0.532	(6)	DFSS	81We
			108	-0.394	(5)	DFSS	81We
			110	-0.256	(4)	DFSS	81We
			112	-0.121	(3)	DFSS	81We
			114	0		DFSS	81We
			116	0.096	(1)	DFSS	81We

El	Z	A°	A	$\delta\langle r^2\rangle^{AA'}$ (fm^2)		Method	References
In	49	115	107	-0.590	(10)	LS	85U1
			108	-0518	(9)	LS	85U1
			109	-0.421	(7)	LS	85U1
			110m	-0.371	(8)	LS	85U1
			113	-0.131	(3)	LS	85U1
			115	0		LS	85U1
Sn	50	120	112	-0.497	(13)	LS	83Ba
			114	-0.366	(11)	LS	83Ba
			115	-0.322	(10)	LS	83Ba
			116	-0.236	(7)	LS	83Ba
			117	-0.188	(8)	LS	83Ba
			118	-0.112	(5)	LS	83Ba
			119	-0.068	(7)	LS	83Ba
			120	0		LS	83Ba
			122	0.100	(5)	LS	83Ba
			124	0.191	(7)	LS	83Ba
Cs	55	133	118	-0.505	(6)	LS	81Th2
			119	-0.136	(3)	LS	81Th2
			119m	-0.334	(4)	LS	81Th2
			120	-0.1185	(14)	LS	81Th2
			121	-0.2555	(9)	LS	81Th2
			121m	-0.0702	(8)	LS	81Th2
			122	-0.2524	(15)	LS	81Th2

El	Z	A'	A	$\delta\langle r^2\rangle^{AA'}$ (fm^2)		Method	References
Cs	55	133	122m	-0.0681	(18)	LS	81Th2
			123	-0.2078	(6)	LS	81Th2
			124	-0.2008	(12)	LS	81Th2
			125	-0.1517	(6)	LS	81Th2
			126	-0.1586	(9)	LS	81Th2
			127	-0.0985	(7)	LS	81Th2
			128	-0.1131	(4)	LS	81Th2
			129	-0.0561	(10)	LS	81Th2
			130	-0.0465	(10)	LS	81Th2
			130m	-0.0628	(14)	LS	81Th2
			131	-0.0141	(7)	LS	81Th2
			132	-0.0369	(6)	LS	81Th2
			133	0		LS	81Th2
			134	-0.0096	(11)	LS	81Th2
			134m	0.0037	(16)	LS	81Th2
			135	0.0250	(9)	LS	81Th2
			135m	0.0169	(10)	LS	81Th2
			136	0.0168	(14)	LS	81Th2
			136m	0.0743	(15)	LS	81Th2
			137	0.0821	(11)	LS	81Th2
			138	0.2023	(8)	LS	81Th2
			139	0.3604	(12)	LS	81Th2
			140	0.4869	(13)	LS	81Th2
			141	0.6159	(14)	LS	81Th2
			142	0.7454	(7)	LS	81Th2

El	Z	A'	A	$\delta\langle r^2\rangle^{AA'}$ (fm^2)		Method	References
Cs	55	133	143	0.8798	(5)	LS	81Th2
			144	0.9669	(7)	LS	81Th2
			145	1.0953	(10)	LS	81Th2
Ba	56	138	122	-0.204	(2)	LS	83Mu
			123	-0.220	(3)	LS	83Mu
			124	-0.175	(1)	LS	83Mu
			125	-0.182	(2)	LS	83Mu
			126	-0.142	(1)	LS	83Mu
			127	-0.158	(2)	LS	83Mu
			128	-0.111	(1)	LS	83Mu
			129	-0.118	(1)	LS	83Mu
			129m	-0.130	(1)	LS	83Mu
			130	-0.086	(1)	LS	83Mu
			131	-0.093	(1)	LS	83Mu
			131m	-0.096	(1)	LS	83Mu
			132	-0.068	(1)	LS	83Mu
			133	-0.084	(1)	LS	83Mu
			133m	-0.072	(1)	LS	83Mu
			134	-0.053	(1)	LS	83Mu
			135	-0.079	(1)	LS	83Mu
			136	-0.041	(1)	LS	83Mu
			137	-0.059	(1)	LS	83Mu
			137m	0.004	(1)	LS	83Mu
			138	0		LS	83Mu

El	Z	A'	A	$\delta\langle r^2\rangle^{AA'}$ (fm^2)		Method	References
Ba	56	138	139	0.124	(1)	LS	83Mu
			140	0.281	(1)	LS	83Mu
			141	0.395	(2)	LS	83Mu
			142	0.529	(1)	LS	83Mu
			143	0.654	(1)	LS	83Mu
			144	0.793	(1)	LS	83Mu
			145	0.893	(1)	LS	83Mu
			146	1.019	(1)	LS	83Mu
Sm	62	148	144	-0.517	(27)	LS	80Br1
			146	-0.251	(29)	LS	80Br1
			147	-0.152	(8)	LS	80Br1
			148	0		LS	80Br1
			149	0.092	(5)	LS	80Br1
			150	0.303	(16)	LS	80Br1
			151	0.464	(29)	LS	80Br1
			152	0.726	(27)	LS	80Br1
			154	0.956	(30)	LS	80Br1
Eu	63	145	140	0.033	(12)	LS	85Ah
			141	0.035	(9)	LS	85Ah
			142	-0.054	(10)	LS	85Ah
			142m	0.003	(6)	LS	85Ah
			143	-0.026	(5)	LS	85Ah
			144	-0.0050	(6)	LS	85Ah

El	Z	A°	A	$\delta\langle r^2\rangle^{AA'}$ (fm^2)		Method	References
Eu	63	145	145	0		LS	85Ah
			146	0.124	(9)	LS	85Ah
			147	0.271	(17)	LS	85Ah
			148	0.376	(24)	LS	85Ah
			149	0.532	(33)	LS	85Ah
			150	0.625	(39)	LS	85Ah
			150m	0.634	(40)	LS	85Ah
			151	0.851	(51)	LS	85Ah
			152	1.396	(81)	LS	85Ah
			153	1.453	(83)	LS	85Ah
Gd	64	154	154	0		MUXR	83La
			155	0.096	(25)	MUXR	83La
			156	0.216	(25)	MUXR	83La
			157	0.248	(27)	MUXR	83La
			158	0.385	(27)	MUXR	83La
			160	0.546	(27)	MUXR	83La
Er	68	162	162	0.503	(45)	LS	85Be
			164	0.359	(32)	LS	85Be
			166	0.240	(22)	LS	85Be
			167	0.199	(18)	LS	85Be
			168	0.121	(10)	LS	85Be
			170	0		LS	85Be

El	Z	A'	A	$\delta\langle r^2\rangle^{AA'}$ (fm^2)		Method	References
Yb	70	168	158	-0.9554	(58)	LS	82Bu
			160	-0.7319	(38)	LS	82Bu
			161	-0.6472	(32)	LS	82Bu
			162	-0.5157	(28)	LS	82Bu
			163	-0.4340	(23)	LS	82Bu
			164	-0.3135	(27)	LS	82Bu
			165	-0.2409	(16)	LS	82Bu
			166	-0.1397	(10)	LS	82Bu
			167	-0.0640	(5)	LS	82Bu
			168	0		LS	82Bu
			169	0.0517	(14)	LS	82Bu
			170	0.1173	(12)	LS	79Cl
			171	0.1573	(14)	LS	79Cl
			172	0.2279	(19)	LS	79Cl
			173	0.2664	(23)	LS	79Cl
			174	0.3144	(27)	LS	79Cl
			176	0.3968	(34)	LS	79Cl
Os	76	188	186	-0.104	(4)	MUXR	81Ho
			188	0		MUXR	81Ho
			190	0.090	(4)	MUXR	81Ho
			192	0.175	(5)	MUXR	81Ho
Au	79	197	190	0.261	(12)	RFS	85St
			191	0.227	(5)	RFS	85St

El	Z	A'	A	$\delta\langle r^2\rangle^{AA'}$ (fm^2)		Method	References
Au	79	197	192	0.195	(5)	RFS	85St
			193	0.148	(4)	RFS	85St
			195	0.072	(6)	RFS	85St
			197	0		RFS	85St
Hg	80	204	181	-0.471	(6)	BRDOP	76Bo
			183	-0.420	(5)	BRDOP	76Bo
			185	-0.429	(4)	BRDOP	76Bo
			187	-0.850	(4)	BRDOP	76Bo
			189	-0.782	(4)	BRDOP	76Bo
			191	-0.698	(5)	BRDOP	76Bo
			192	-0.629	(6)	BRDOP	76Bo
			193	-0.599	(3)	BRDOP	76Bo
			193m	-0.590	(3)	BRDOP	76Bo
			194	-0.533	(2)	BRDOP	76Bo
			195	-0.486	(2)	BRDOP	76Bo
			195m	-0.492	(3)	BRDOP	76Bo
			196	-0.435	(3)	BRDOP	76Bo
			197	-0.404	(4)	BRDOP	76Bo
			197m	-0.392	(3)	BRDOP	76Bo
			198	-0.343	(1)	BRDOP	76Bo
			199	-0.328	(1)	BRDOP	76Bo
			199m	-0.271	(3)	BRDOP	76Bo
			200	-0.235	(1)	BRDOP	76Bo
			201	-0.199	(1)	BRDOP	76Bo

El	Z	A'	A	$\delta\langle r^2\rangle^{AA'}$ (fm^2)		Method	References
Hg	80	204	202	-0.117	(1)	BRDOP	76Bo
			203	-0.080	(4)	BRDOP	76Bo
			204	0		BRDOP	76Bo
			205	0.040	(2)	BRDOP	76Bo
Pb	82	208	198	-0.527	(12)	LS	83Th
			199	-0.5175	(54)	LS	83Th
			200	-0.4320	(72)	LS	83Th
			201	-0.4094	(41)	LS	83Th
			202	-0.3298	(44)	LS	83Th
			202m	-0.3316	(42)	LS	83Th
			203	-0.3033	(35)	LS	83Th
			204	-0.2237	(25)	LS	83Th
			205	-0.1946	(40)	LS	83Th
			206	-0.1176	(13)	LS	83Th
			207	-0.0723	(25)	LS	83Th
			208	0		LS	83Th
			209	0.0905	(52)	LS	83Th
			210	0.202	(14)	LS	83Th
			212	0.399	(27)	LS	83Th
Fr	87	212	207	-0.08892	(7)	LS	85Co
			208	-0.08484	(5)	LS	85Co
			209	-0.05317	(3)	LS	85Co
			210	-0.04413	(2)	LS	85Co

El	Z	A'	A	$\delta\langle r^2\rangle^{AA'}$ (fm^2)	Method	References
Fr	87	212	211	-0.01530 (5)	LS	85Co
			212	0	LS	85Co
			213	0.02780 (3)	LS	85Co
			220	0.35207 (1)	LS	85Co
			221	0.39881 (3)	LS	85Co
			222	0.44436 (5)	LS	85Co
			223	0.47247 (3)	LS	85Co
			224	0.52269 (2)	LS	85Co
			225	0.54651 (2)	LS	85Co
			226	0.58212 (2)	LS	85Co
			227	0.64892 (3)	LS	85Co
			228	0.67813 (8)	LS	85Co

TABLE III. Magnetic Dipole Moments, spins and Electric Quadrupole Moments Isotopes.

El	A	$\mu(\mu_N)$		I	Q_s	Method	Refs
Na	21	2.38612	(10)	3/2		HFS	78Hu
	22	1.746	(3)	3		HFS	78Hu
	23	2.217520	(2)	3/2		HFS	78Hu
	24	1.6902	(5)	4		HFS	78Hu
	25	3.683	(4)	5/2		HFS	78Hu
	26	2.851	(2)	3		HFS	78Hu
	27	3.895	(5)	5/2		HFS	78Hu
	28	2.426	(3)	1		HFS	78Hu
	29	2.449	(8)	3/2		HFS	78Hu
	30	2.083	(10)	2		HFS	78Hu
	31	2.283	(38)	3/2		HFS	78Hu
K	38	1.371	(6)	3		HFS	82To
	39	0.391466		3/2		HFS	82To
	40	-1.2982	(4)	4		HFS	82To
	41	0.214870		3/2		HFS	82To
	42	-1.1425	(6)	2		HFS	82To
	43	0.1633	(8)	3/2		HFS	82To
	44	-0.856	(4)	2		HFS	82To
	45	0.1734	(8)	3/2		HFS	82To
	46	-1.051	(6)	2		HFS	82To
	47	1.933	(9)	1/2		HFS	82To
Ca	41	-1.606	(20)	7/2		HFS	82An
	43	-1.3172	(6)	7/2		HFS	82An
	45	-1.316	(16)	7/2		HFS	82An
	47	-1.380	(24)	7/2		HFS	82An
Rb	76	-0.376	(9)	1	0.38 (15)	HFS	81Th1
	77	0.6568	(41)	3/2	0.695 (32)	HFS	81Th1

El	A	$\mu(\nu_{ph})$		I	Q_s		Method	Refs
Rb	78m	2.5485	(21)	4	0.814	(39)	HFS	81Thl
	79	3.3579	(12)	5/2	-0.098	(22)	HFS	81Thl
	80	-0.0833	(17)	1	-0.348	(20)	HFS	81Thl
	81	2.0595	(14)	3/2	0.398	(23)	HFS	81Thl
	81m	5.5980	(17)	9/2	-0.743	(57)	HFS	81Thl
	82	0.5536	(54)	1	0.190	(72)	HFS	81Thl
	82m	1.5133	(24)	5	1.01	(12)	HFS	81Thl
	83	1.4249	(8)	5/2	0.196	(22)	HFS	81Thl
	84	-1.3246	(16)	2	-0.015	(35)	HFS	81Thl
	84m	0.220	(15)	6	0.57	(27)	HFS	81Thl
	85	1.3570	(10)	5/2	0.228	(43)	HFS	81Thl
	86	-1.6977	(16)	2	0.193	(32)	HFS	81Thl
	86m	1.018	(10)	6	0.369	(95)	HFS	81Thl
	87	2.7506	(10)	3/2	0.130	(21)	HFS	81Thl
	88	0.5117	(26)	2	-0.012	(96)	HFS	81Thl
	89	2.3836	(7)	3/2	0.144	(26)	HFS	81Thl
	90m	1.61598	(64)	3	0.204	(45)	HFS	81Thl
	91	2.1815	(15)	3/2	0.154	(26)	HFS	81Thl
	93	1.4095	(16)	5/2	0.177	(40)	HFS	81Thl
	94	1.4984	(18)	3	0.163	(50)	HFS	81Thl
	95	1.3336	(34)	5/2	0.211	(65)	HFS	81Thl
	96	1.4658	(17)	2	0.246	(56)	HFS	81Thl
	97	1.8410	(21)	3/2	0.581	(44)	HFS	81Thl
Ag	107	-0.113		1/2			HFS	75Fu
	108m	3.577	(20)	6	1.52	(8)	HFS	75Fi
	109	-0.130		1/2			HFS	75Fu
	110m			6	1.65	(10)	HFS	75Fi
In	113	5.496		9/2			HFS	75Fu
	115	5.5077		9/2			HFS	75Fu
Sb	121	3.360		5/2			HFS	75Fu
	123	2.5484		7/2			HFS	75Fu

El	A	$\mu(\mu_N)$		I	Q_s		Method	Refs
Cs	118	4.29	(10)	2	1.9	(3)	HFS	81Th2
	119	5.46	(3)	9/2	2.8	(1)	HFS	81Th2
	119m	0.838	(5)	3/2	0.9	(1)	HFS	81Th2
	120	3.87	(2)	2	1.45	(2)	HFS	81Th2
	121	0.770	(14)	3/2	0.838	(9)	HFS	81Th2
	121m	5.41	(3)	9/2	2.69	(5)	HFS	81Th2
	122	-0.1333	(9)	1	-0.19	(1)	HFS	81Th2
	122m	4.77	(2)	8	3.29	(8)	HFS	81Th2
	123	1.377	(7)	1/2	-0.74	(3)	HFS	81Th2
	124	0.673	(3)	1	-0.68	(2)	HFS	81Th2
	125	1.409	(7)	1/2			HFS	81Th2
	126	0.777	(4)	1	-0.68	(2)	HFS	81Th2
	127	1.459	(7)	1/2			HFS	81Th2
	128	0.974	(5)	1	-0.570	(8)	HFS	81Th2
	129	1.491	(8)	1/2			HFS	81Th2
	130	1.460	(7)	1	-0.059	(6)	HFS	81Th2
	130m	0.629	(4)	5	1.45	(5)	HFS	81Th2
	131	3.53	(2)	5/2	-0.67	(4)	HFS	81Th2
	132	2.23	(1)	2	0.49	(2)	HFS	81Th2
	133			7/2	-0.009	(4)	HFS	81Th2
	134	2.99	(2)	4	0.38	(4)	HFS	81Th2
	134m	1.111	(6)	8	0.98	(8)	HFS	81Th2
	135	2.73	(1)	7/2	0.03	(2)	HFS	81Th2
	135m	2.18	(1)	19/2	0.89	(7)	HFS	81Th2
	136	3.71	(2)	5	0.17	(6)	HFS	81Th2
	136m	1.319	(7)	8	0.74	(10)	HFS	81Th2
	137	2.84	(1)	7/2	0.03	(4)	HFS	81Th2
	138	0.700		3	0.12	(2)	HFS	81Th2
	138m	1.713	(9)	6	-0.40	(3)	HFS	81Th2
	139	2.70	(1)	7/2	-0.06	(1)	HFS	81Th2
	140	0.134	(1)	1	-0.10	(2)	HFS	81Th2
	141	2.41	(1)	7/2	-0.45	(7)	HFS	81Th2
	143	0.870	(3)	3/2	0.47	(3)	HFS	81Th2
	144	-0.546	(3)	1	0.30	(1)	HFS	81Th2
	145	0.784	( )	3/2	0.62	(6)	HFS	81Th2

El	A	$\mu(\mu_N)$		I	Q_s		Method	Refs
Ba	123	-0.687	(18)	5/2	1.52	(13)	HFS	83Mu
	125	0.177	(12)	1/2			HFS	83Mu
	127	0.089	(12)	1/2			HFS	83Mu
	129	-0.398	(16)	1/2			HFS	83Mu
		-0.397	(6)	1/2			HFS	79Be
	129m	0.930	(17)	7/2	1.60	(13)	HFS	83Mu
		0.928	(5)		1.94	(3)	HFS	79Be
	131	-0.709	(16)	1/2			HFS	83Mu
		-0.707	(6)	1/2			HFS	79Be
	131m	-0.870	(18)	9/2	1.46	(13)	HFS	83Mu
	133	-0.777	(14)	1/2			HFS	83Mu
		-0.776	(2)	1/2			HFS	79Be
	133m	-0.910	(51)	11/2	0.89	(7)	HFS	83Mu
		-0.910	(40)	11/2			HFS	79Be
	135	0.837943	(17)	3/2	0.146	(16)	HFS	83Mu
		0.83656	(2)	3/2			HFS	79Be
	135m	-1.001	(15)	11/2	0.96	(8)	HFS	83Mu
		-0.999	(2)	11/2			HFS	79Be
	137	0.937365	(20)	3/2	0.228	(24)	HFS	83Mu
		0.93582	(2)		0.28	(3)	HFS	79Be
	137m	-0.992	(26)	1/2	0.78	(9)	HFS	83Mu
	139	-0.975	(17)	7/2	0.50	(4)	HFS	83Mu
	141	-0.346	(16)	3/2	0.43	(4)	HFS	83Mu
	143	0.454		5/2	-0.81	(7)	HFS	83Mu
	145	-0.380	(25)	(3/2)	0.81	(7)	HFS	83Mu
Gd	155			3/2	1.27	(3)	HFS	83La
	157			3/2	1.35	(3)	HFS	83La
Eu	140	1.365	(13)	1	0.31	(4)	HFS	85Ah
	141	3.494	(8)	5/2	0.85	(4)	HFS	85Ah
	142	1.536	(19)	1	0.12	(5)	HFS	85Ah
	142m	2.978	(11)	8	1.41	(6)	HFS	85Ah

El	A	$\mu(\mu_N)$		I	Q_s		Method	Refs
Eu	143	3.673	(8)	5/2	0.51	(3)	HFS	85Ah
	144	1.893	(13)	1	0.10	(3)	HFS	85Ah
	145	3.993	(7)	5/2	0.29	(2)	HFS	85Ah
	146	1.425	(11)	4	-0.18	(6)	HFS	85Ah
	147	3.724	(8)	5/2	0.55	(3)	HFS	85Ah
	148	2.340	(10)	5	0.35	(6)	HFS	85Ah
	149	3.565	(6)	5/2	0.75	(2)	HFS	85Ah
	150	2.708	(11)	5	1.13	(5)	HFS	85Ah
	151	3.4717	(6)	5/2	0.95	(3)	HFS	85Ah
	152	-1.96	(6)	3	2.54	(22)	HFS	85Ah
	153	1.538	(13)	5/2	2.412	(21)	HFS	85Ah
Yb	169	-0.63	(2)	7/2	4.10	(6)	HFS	74Ch
Au	197	0.14486		3/2			HFS	75Fu
	198	0.590		2			HFS	75Fu
Hg	181	0.5071	(7)	1/2			HFS	76Bo
	183	0.524	(5)	1/2			HFS	76Bo
	185	0.507	(4)	1/2			HFS	76Bo
	185m	-1.07	(7)	13/2	0.9	(17)	HFS	79Da
	187	-0.593	(4)	3/2	-0.50	(23)	HFS	76Bo
	187m	-1.044	(11)	13/2	0.55	(35)	HFS	79Da
	189	-0.6086	(7)	3/2	-1.15	(25)	HFS	76Bo
	189m	-1.058	(6)	13/2	0.78	(24)	HFS	79Da
	191			3/2	-0.41	(41)	HFS	76Bo
	191m	-1.068	(5)	13/2	0.76	(24)	HFS	79Da
	193	-0.62757	(18)	3/2	-0.86	(38)	HFS	76Bo
	193m	-1.058429	(3)	13/2	1.08	(10)	HFS	76Bo
	195	0.541475	(1)	1/2	1.08	(10)	HFS	76Bo
	195m	-1.044647	(3)	1/2	1.27	(11)	HFS	76Bo
	197	0.5273741	(9)	1/2			HFS	76Bo
	197m	-1.027684	(3)	13/2	1.47	(13)	HFS	76Bo

El	A	$\mu(\mu_N)$	I	Q_s	Method	Refs
Hg	199	0.5058852(9)	1/2		HFS	76Bo
	199m	-1.014703 (3)	13/2	1.40 (42)	HFS	76Bo
	201	-0.560225 (1)	3/2	0.455 (40)	HFS	76Bo
	203	0.84895 (13)	5/2	0.40 (4)	HFS	76Bo
	205	0.6009 (1)	1/2		HFS	76Bo
Pb	199	-1.048 (21)	3/2	0.05 (5)	HFS	83Th
	201	0.659 (13)	5/2	-0.01 (5)	HFS	83Th
	202m	-0.222 (4)	9	0.36 (8)	HFS	83Th
	203	0.670 (13)	5/2	0.06 (5)	HFS	83Th
	205	0.695 (14)	5/2	0.14 (3)	HFS	83Th
	207	0.5783	1/2		HFS	83Th
	209	-1.438	9/2	-0.16 (10)	HFS	83Th
Tl	203	1.5962	1/2		HFS	75Fu
	205	1.6118	1/2		HFS	75Fu
Fr	207	3.89 (8)	9/2	-0.16 (5)	HFS	85Co
	208	4.75 (2)	7	0.004 (38)	HFS	85Co
	209	3.95 (2)	9/2	-0.24 (2)	HFS	85Co
	210	4.40 (9)	6	0.19 (2)	HFS	85Co
	211	4.00 (8)	9/2	-0.19 (3)	HFS	85Co
	212	4.62 (9)	5	-0.10 (1)	HFS	85Co
	213	4.02 (1)	9/2	-0.14 (2)	HFS	85Co
	220	-0.67 (1)	1	0.482 (2)	HFS	85Co
	221	1.58 (3)	5/2	-1.00 (1)	HFS	85Co
	222	0.63 (1)	2	0.51 (4)	HFS	85Co
	223	1.17 (2)	3/2	1.17 (1)	HFS	85Co
	224	0.40 (1)	1	0.517 (4)	HFS	85Co
	225	1.07 (2)	3/2	1.32 (1)	HFS	85Co
	226	0.071 (2)	1	-1.35 (2)	HFS	85Co
	227	1.50 (3)	1/2		HFS	85Co
	228	-0.76 (2)	2	2.38 (5)	HFS	85Co

El	A	$\mu(\mu_N)$		I	Q_s		Method	Refs
Ra	211	0.90	(5)	5/2	0.45	(7)	HFS	83Ah
	213	0.62	(3)	1/2			HFS	83Ah
	221	-0.18	(1)	5/2	1.9	(3)	HFS	83Ah
	223	0.28	(2)	3/2	1.2	(2)	HFS	83Ah
	225	-0.75	(4)	1/2			HFS	83Ah
	227	-0.41	(2)	3/2	1.5	(3)	HFS	83Ah
	229	0.51	(3)	5/2	2.9	(5)	HFS	83Ah

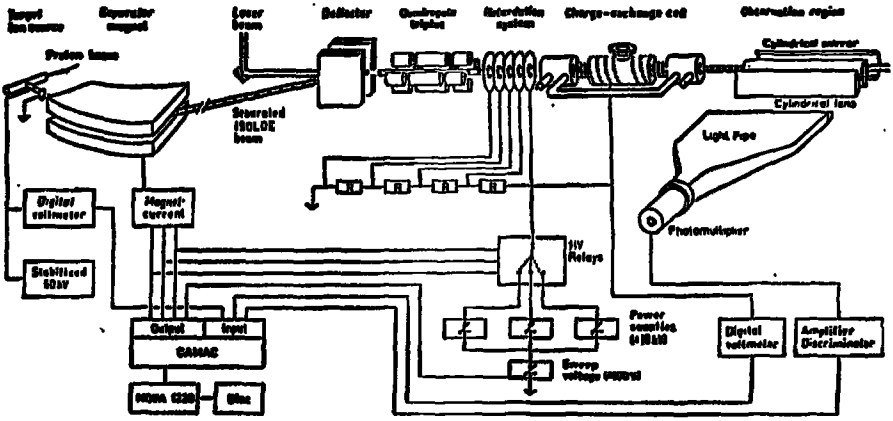

Figure I : Schema of Collinear Fast-beam Laser Spectroscopy Connected to the On-line ISOLDE Separator (83Mu). Nuclear spins, isotope shifts, magnetic dipole and electric quadrupole moments, and deformation parameters for Ba isotopes had been deduced.

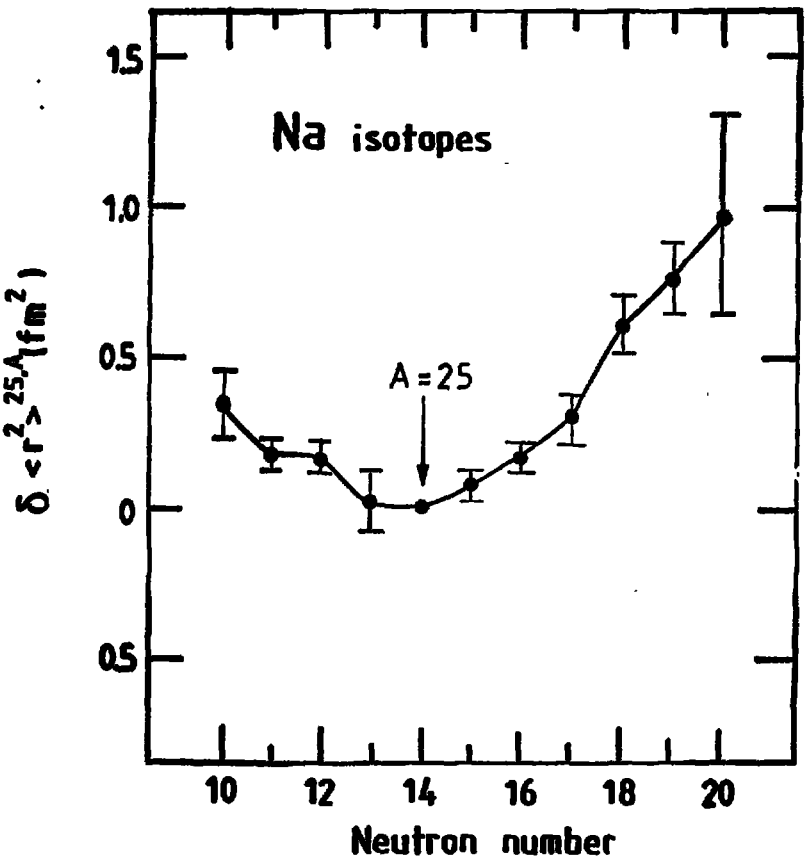

Figure II : Differences of Mean Square Charge Radii with Respect to ^{25}Na(76Hu). The trend of the curve indicates prolate deformation for $^{21-24,28-31}$Na while $^{25-27}$Na may be considered as having almost spherical shapes. Measurements in the neighboring elements Mg and Ne might exhibit a similar structure of the nuclear radius changes.

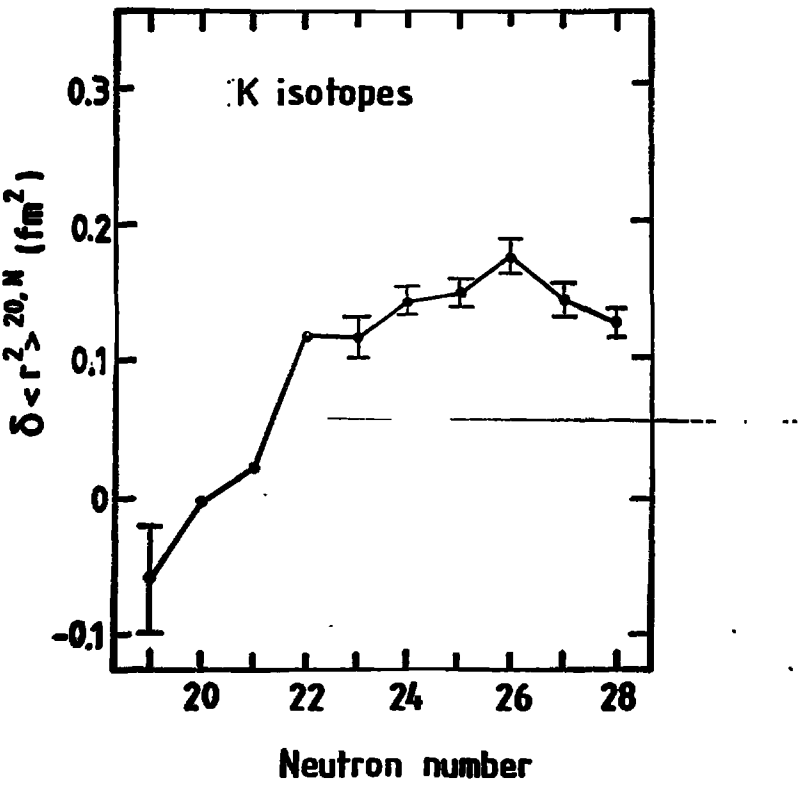

Figure III : Change in the Mean Square Charge Radius in $^{38-47}$K(82To). A shrinking of the charge radii at the end of the filling of the $f_{7/2}$ shell is observed.

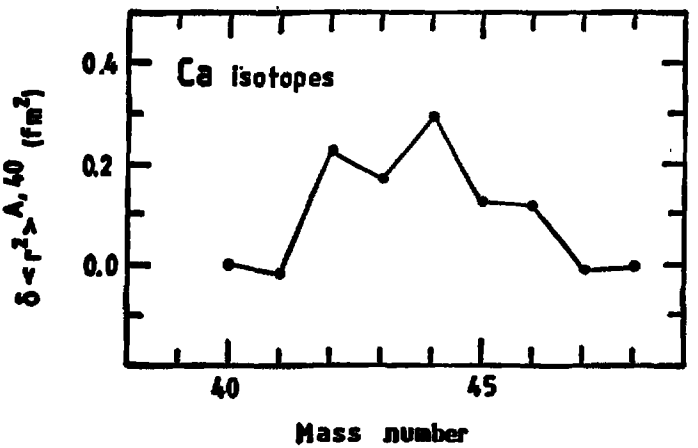

Figure IV : Variation of the Mean Square Charge Radii Differences of Ca Isotopes between the Doubly Magic Nuclei ^{40}Ca and ^{48}Ca(82Am). The normal variation expected for the mean square radius of nuclear charge distribution is an increase with A. The peculiar behaviour of Ca isotopes shows a decrease of $< r^2 >$ while filling up the second half of the neutron shell at N = 28. The rms charge radii of ^{40}Ca and ^{48}Ca are equal within experimental uncertainty, implying that as the $f_{7/2}$ shell is filled, the excess neutrons form a skin outside the ^{40}Ca core. The charge radius of the only stable odd isotope of ^{43}Ca is considerably less than its neighboring even nuclei, implying a partial break up of the first $f_{7/2}$ neutron pair by the additional neutron which form altogether a layer of neutrons around the ^{40}Ca nucleus. There is a distinct odd-even staggering.

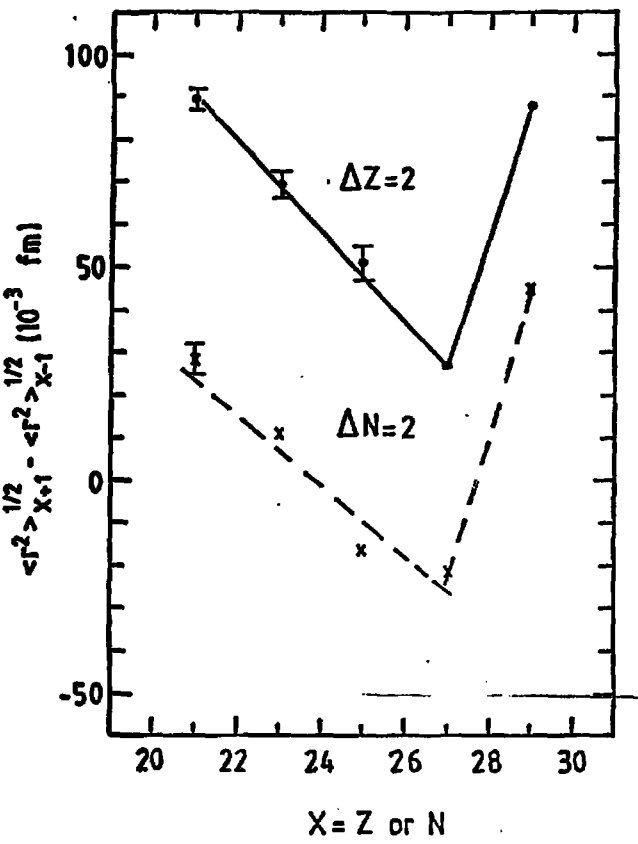

Figure V : Model-independent Isotonic $\Delta Z = 2$ and Isotopic $\Delta N = 2$ Root Mean Square Charge Radii Differences Plotted as Functions of Z or N Respectively (81Mo). Results are deduced from a combined analysis of data from muonic X-ray and elastic electron scattering measurements. Sequential addition of protons to the $f_{7/2}$ orbitals results in a decrease of the successive isotone shifts, independent of the neutron configuration of the nuclei involved. A sudden increase occurs at Z = 28, reflecting the beginning of the $2p_{3/2}$ shell. The sequential addition of neutron pairs to the $f_{7/2}$ orbital causes a decrease in the successive isotope shifts independent of Z, indicating that the added neutrons interact with the entire proton core rather than with the valence protons. An abrupt increase in isotopic shifts occurs at N = 28 indicating the beginning of the $2p_{3/2}$ neutron shell.

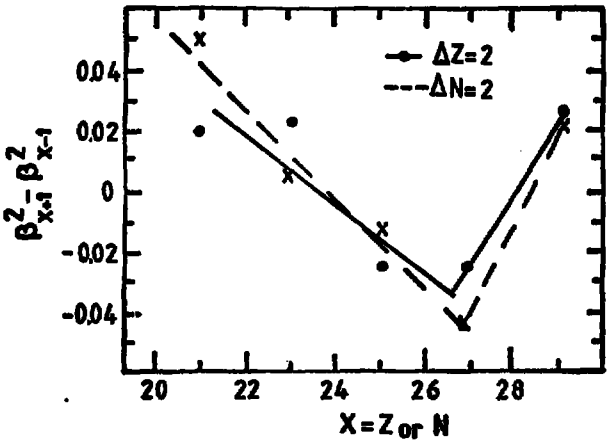

Figure VI : Deformation Changes between ΔZ = 2and ΔN = 2 Pairs of Even $1f_{7/2}$-Shell as Functions of Z or N Respectively (81Mo). A strong conclusion observed between nuclear deformation obtained from B(E2) values and the experimental isotope and isotone shifts, supports the incompressible fluid model at least qualitatively for the $1f_{7/2}$-shell nuclei.

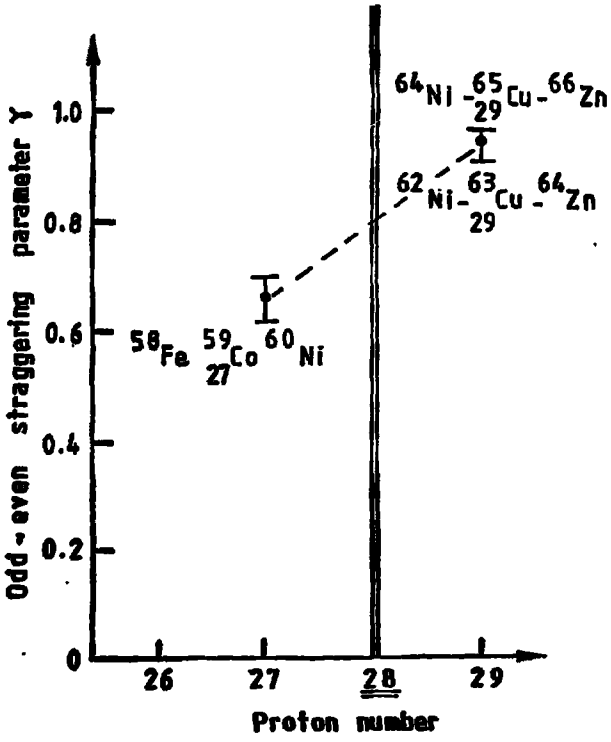

Figure VII : Odd-Even Staggering Parameter γ for Isotones Bracketing the Z = 28 Closed Shell (76 Sh). A large staggering effect observed for ^{59}Co just below Z = 28 and the absence of staggering for both ^{63}Cu and ^{65}Cu just above Z = 28 suggest shell closure at proton number 28.

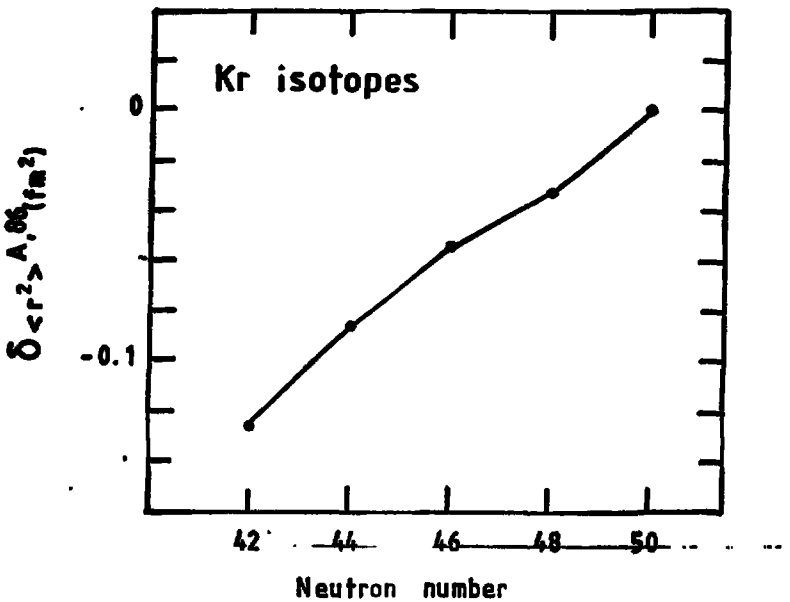

Fig.VIII. Changes in mean square charge distribution differences with reference to A = 86 of Kr isotopes (79Ge)

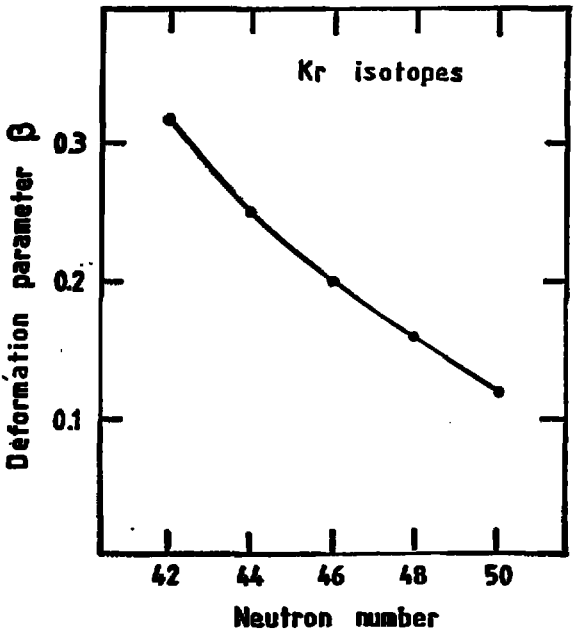

Figure IX : Deformation Parameters β for Even Kr Isotopes versus Neutron Number (79Ge). The nuclear deformation decreases with increasing neutron number, being the smallest for ^{86}Kr with a closed shell at N = 50.

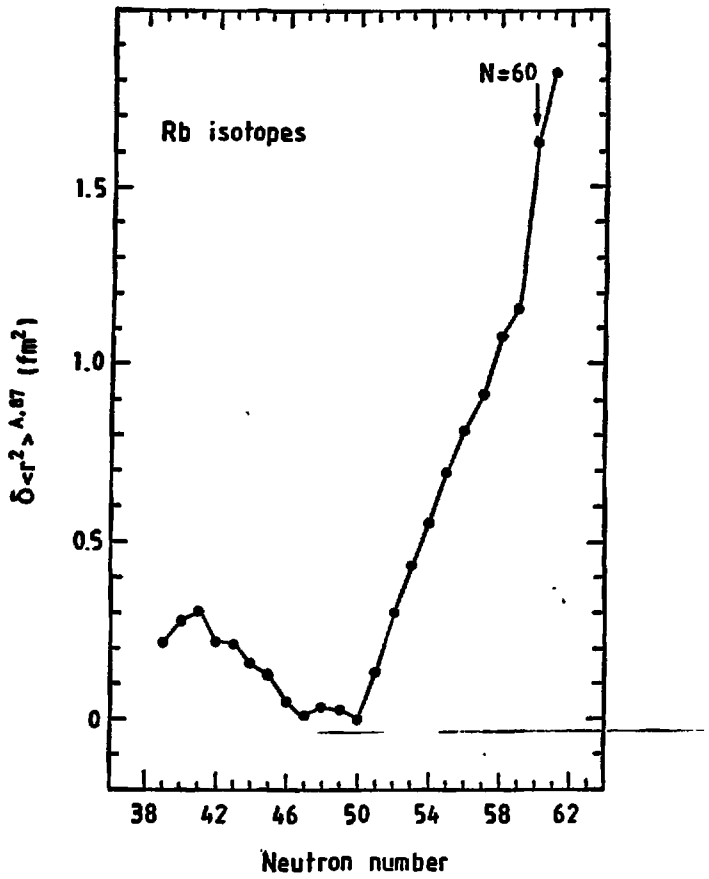

Figure X : Variation of the Mean Square Nuclear Charge Radii Relative to ^{87}Rb(81Th1). From ^{78}Rb to ^{87}Rb, (up to shell closure at N = 50), $\langle r^2 \rangle$ of the nuclear charge distribution decreases when neutrons are added, similar to the trend observed for stable Kr isotopes from N = 42 to 50, reflecting both the charges in volume of the nucleus and departures from spherical symmetry. The curve confirms that $\langle r^2 \rangle$ increases more rapidly when the neutrons start filling a new shell than when the shell is closed. A large purely rotational deformation is seen to arise for N = 60. A strong increase of $\delta \langle r^2 \rangle$ between N = 59 and 60 indicates the onset of deformation for N ≥ 60, an effect which has been confirmed by Rb mass measurements.

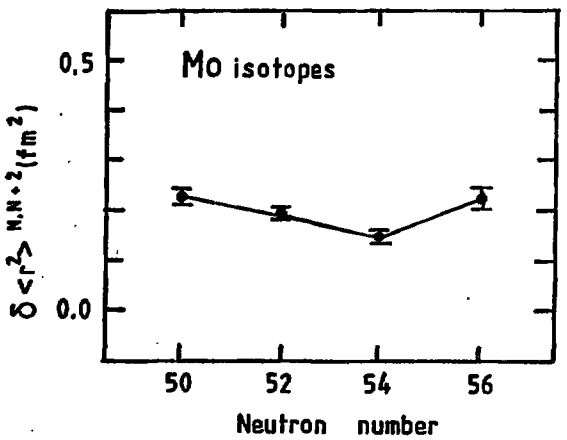

Figure XI : $\delta < r^2 >^{N,N+2}$ as a Function of Neutron Number for Mo Isotopes (78Au). The change in the slope while joining N = 54 and 56 indicates a sub-shell closure at N = 56.

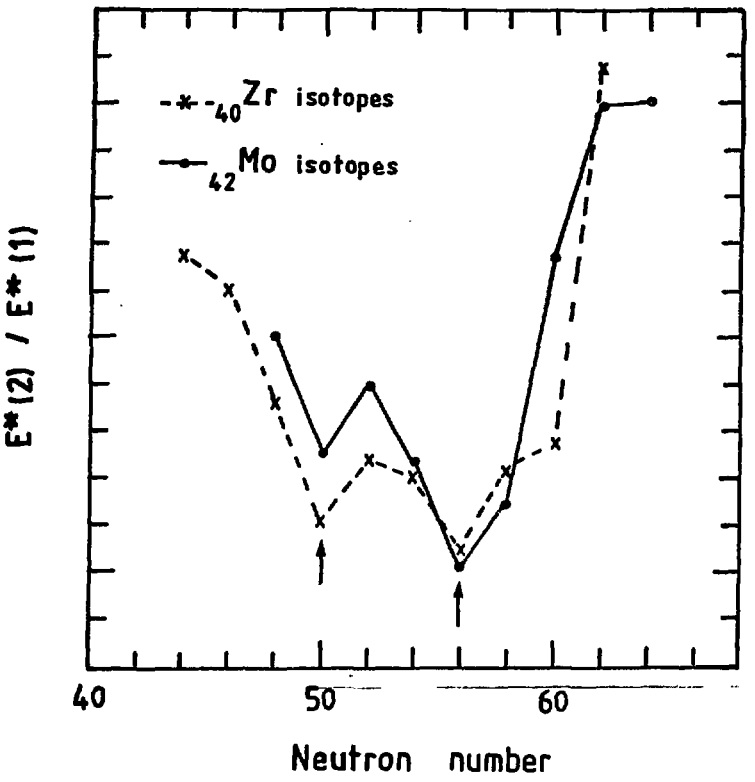

Figure XII : Ratio of $E^*(2)/E^*(1)$ vs Neutron Number for Mo and Zr Isotopes (66An). $E^*(2)$ and $E^*(1)$ are the energies of the second and first excited levels respectively. At the magic neutron number N = 50 and at the sub-shell closure at N = 56, minimum values are observed.

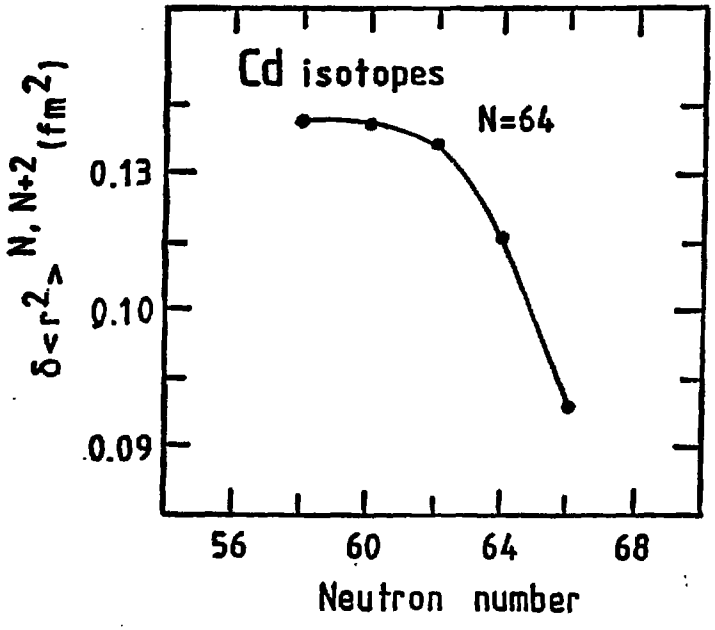

Figure XIII : Trend of $\delta\langle r^2\rangle^{N,N+2}$ for Cd Isotopes with Even Neutron Numbers (81We). A break in the trend of $\delta\langle r^2\rangle$ when passing through N = 64 is attributed to a subshell effect, marking the transition from $d_{5/2}$, $g_{7/2}$ to $s_{1/2}$, $d_{3/2}$ and $h_{11/2}$ neutron orbits.

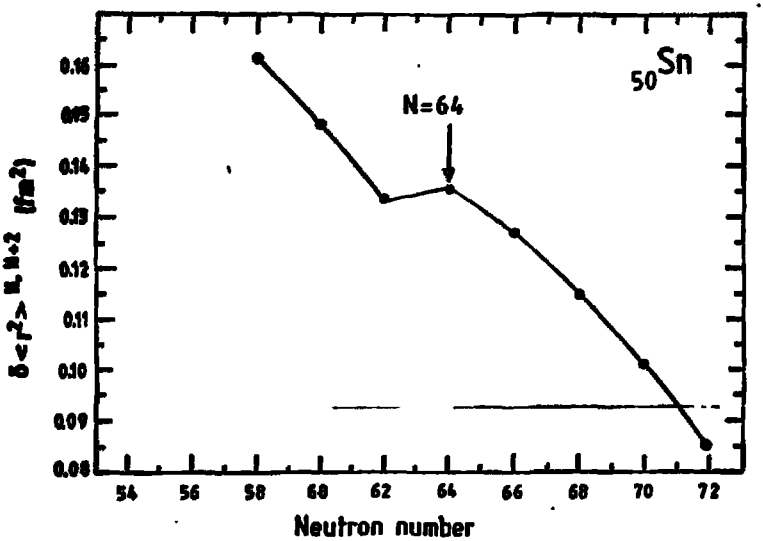

Figure XIV : The Brix-Kopfermann Diagram Representing the Evolution of $\delta < r^2 >^{N,N+2}$ Values of Sn with Even Neutron Numbers (85U1). The change in the slope at N = 62 - 64 might be related to a subshell closure after filling of the $2d_{5/2}$ and $1g_{7/2}$ neutron shells.

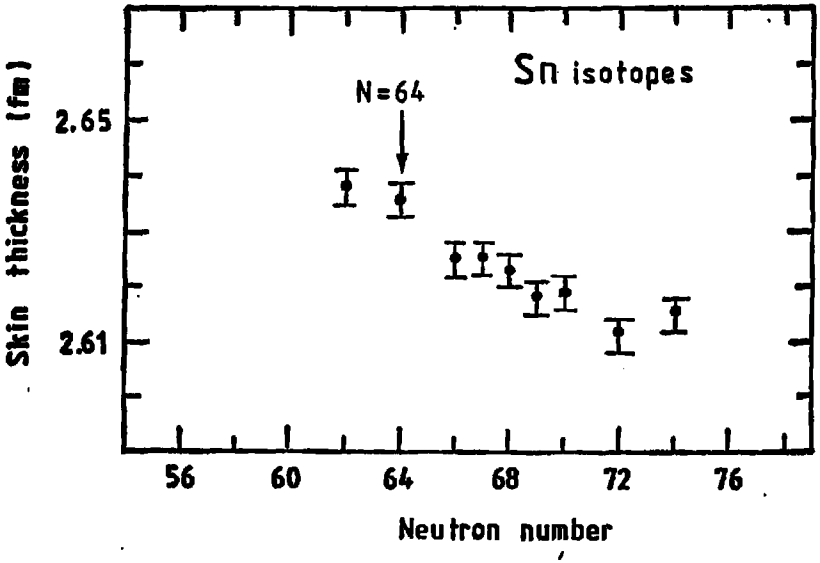

Figure XV : Variation of Reduced Skin Thickness Parameters as a Function of Neutron Number (72Fi). Skin thickness decreases slightly with increasing mass number. A definite change between ^{114}Sn and ^{116}Sn is evidence for the existence of a closed subshell effect at N = 64.

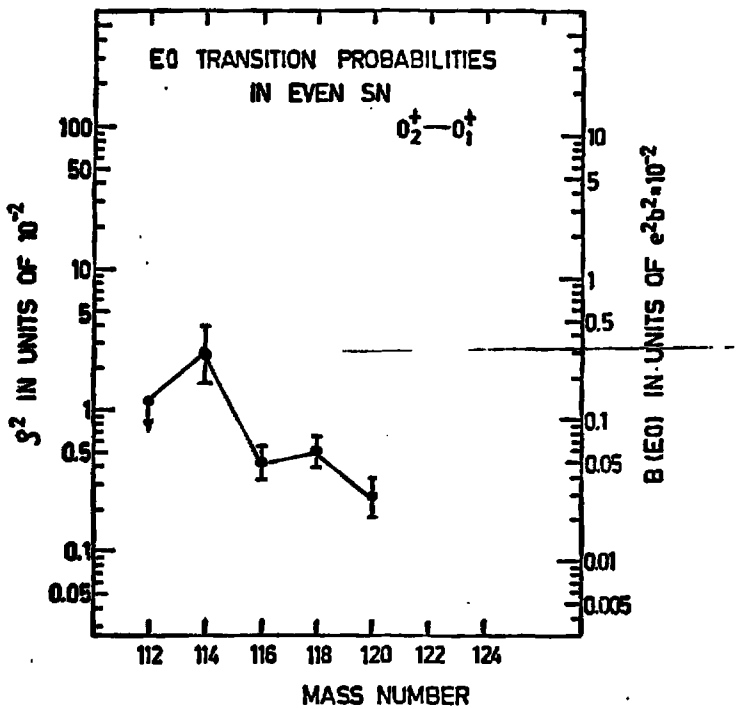

Figure XVI : Monopole Transition Rates in Even Sn Nuclei (81Ba). The sudden jump of E0 transition rates between A = 116 and 114 indicate the closed neutron shell at N = 64.

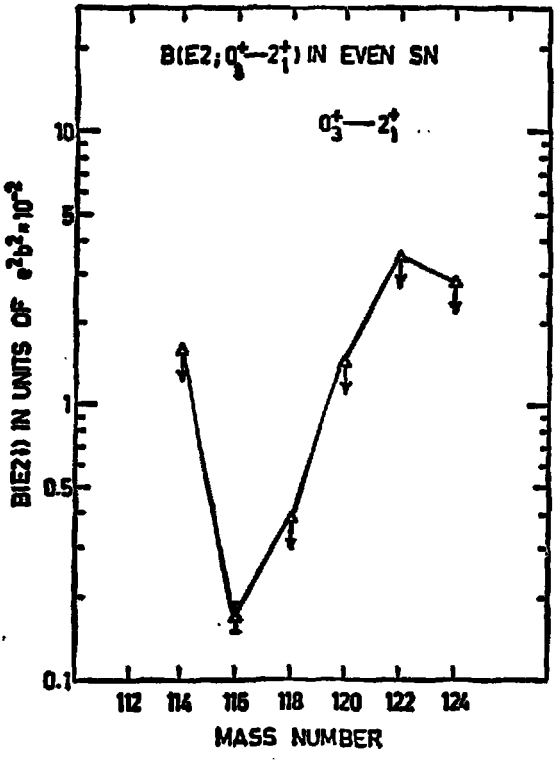

Figure XVII : Reduced E2 Transition Rates in Even Sn Nuclei (81Ba). The E2 systematics show a jump between the mass numbers 116 and 114 indicating closed neutron subshell $d_{5/2} + g_{7/2}$.

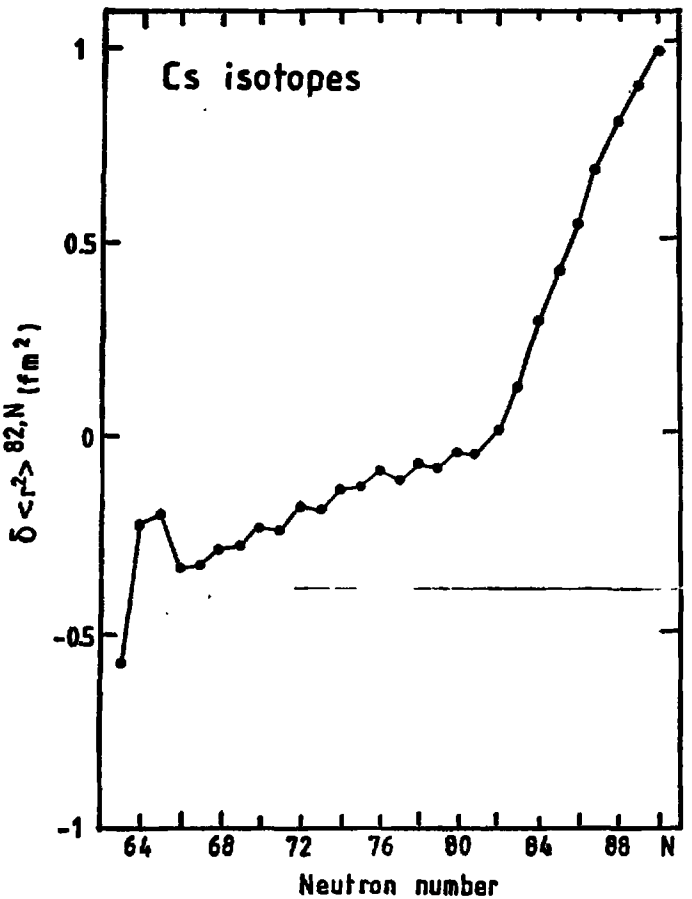

Figure XVIII : Change in the Mean Square Charge Radius Relative to ^{137}Cs(81Th2). Increasingly deformed shapes are observed after the neutron shell closure of N = 82.

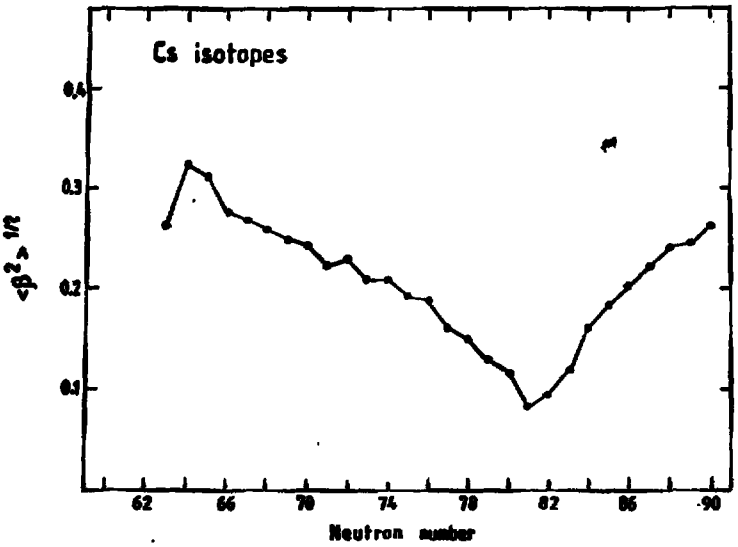

Figure XIX : Values of the Deformation Parameter $< \beta^2 >^{1/2}$ for Cs isotopes(81Th2).

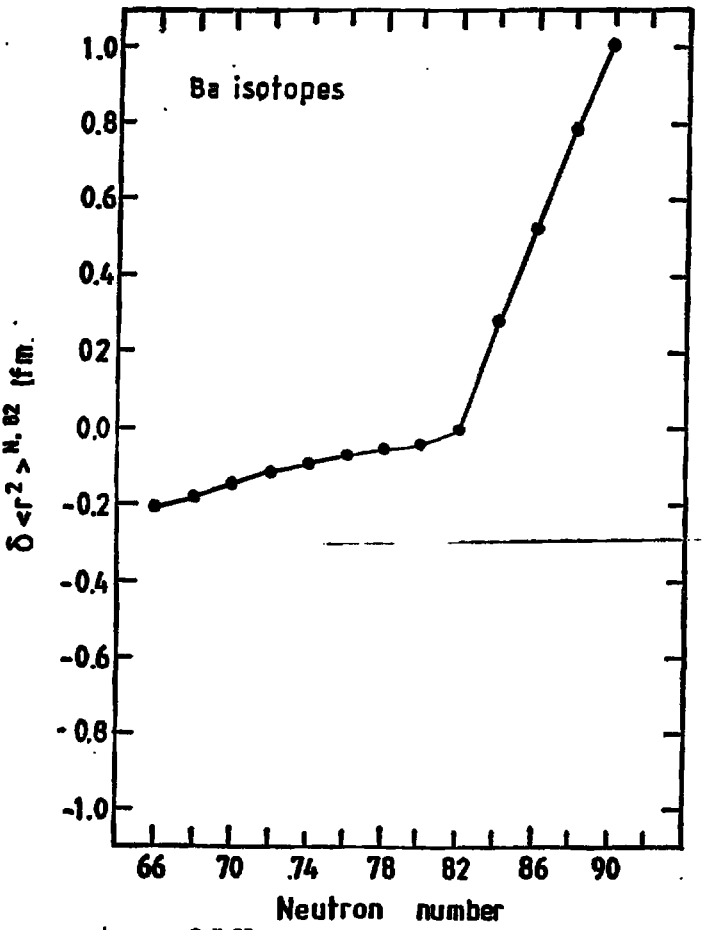

Figure XX : : $\delta < r^2 >^{N,82}$ vs Neutron Number for Ba isotopes (83 Mu). An abrupt change in the gradient, at N = 82 is indicative of the influence of shell structure. The absolute staggering defined as the difference between the odd isotopes and the average of its neighbours is approximately the same for isotopes *with* N < 82 but decreases to zero *within* 82 and 90.

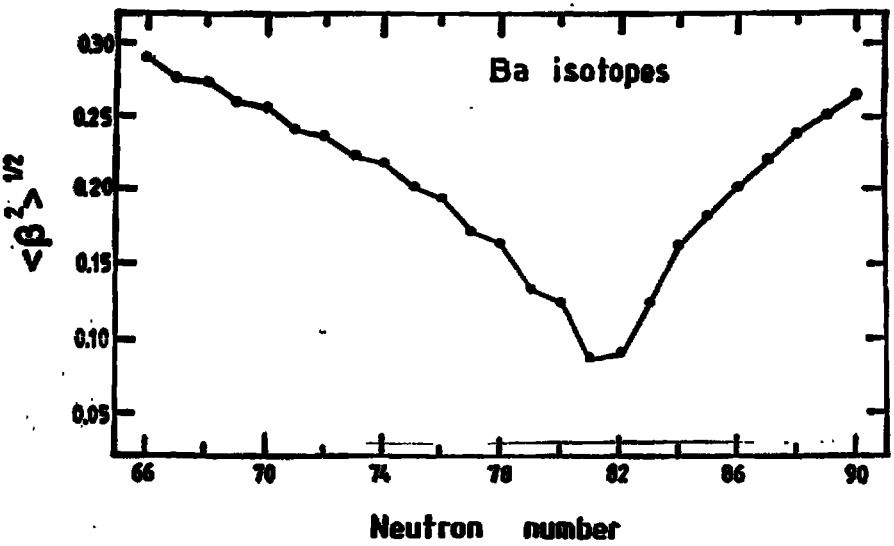

Figure XXI : Plot of Root Mean Square Deformation Parameter $\langle\beta^2\rangle^{1/2}$ Deduced from Isotope Shift Data in the Sequence $^{122-146}$Ba vs Neutron Number (83 Mu). From N = 82 up to N = 90 the curve shows a monotonic increase in $\langle\beta^2\rangle^{1/2}$. For N < 82 the trend continues towards more neutron deficient isotopes.

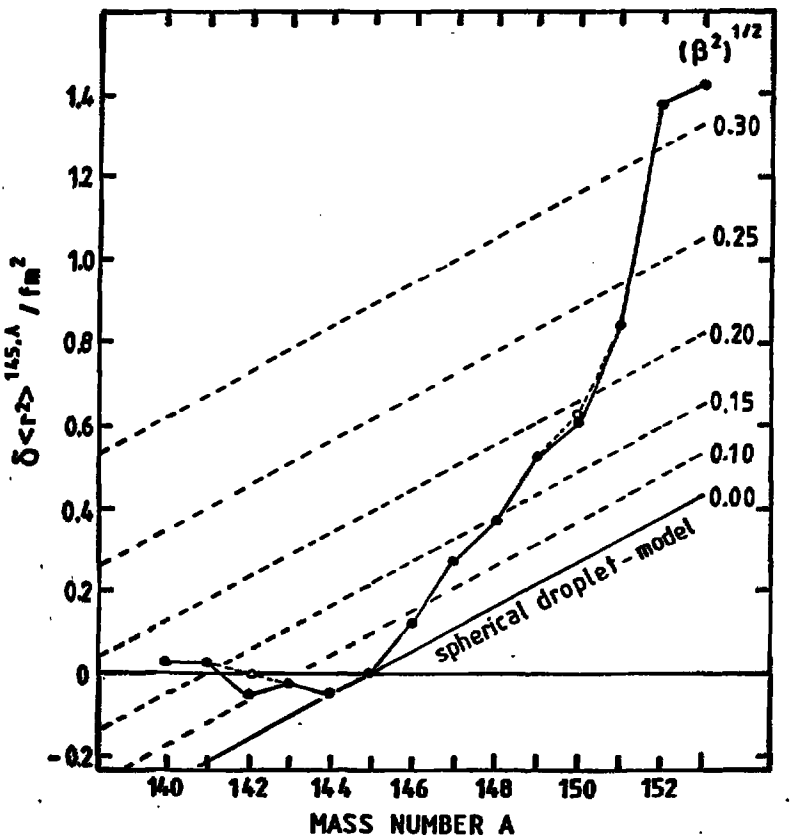

Figure XXII : Plot of $\delta \langle r^2 \rangle^{145,A}$ versus A for the Isotopic Chain $^{140-153}$Eu (85Ah). Except for ^{144}Eu, the observed $\delta < r^2 >$ deviates from the spherical droplet model, indicating deformation developments on both sides of N = 82. The values of $\delta < \beta^2 >^{1/2}$ w.r.t. N = 82 is shown by parallel lines. On the lighter A side, collective effects tend to change $\delta < r^2 >$ of ^{140}Eu(N = 77) and ^{141}Eu (N = 78) compared to ^{145}Eu, while deformation develops as neutrons are added to ^{145}Eu. A steep increase is observed for $88 \leq N \leq 89$, while above 89, in

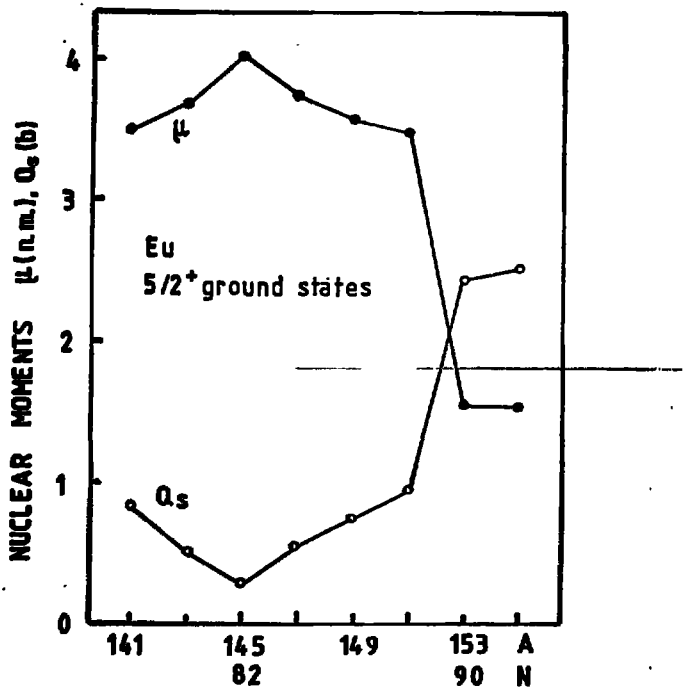

Figure XXIII : Magnetic (μ) and quadrupole (Q_s) Moments of the $5^+/2$ Ground States of Odd A Transitional Nuclei $^{141-151}_{}Eu$ versus Neutron Number(85Ah).These levels are associated with the $2d_{5/2}$ shell-model proton state. The μ plot shows a maximum value at N = 82 and decreasing quantities on either side of it. The nuclear moments of ^{145}Eu can be interpreted in terms of a $(\pi 2d_{5/2})^-$ hole state to a doubly-magic $^{146}_{64}Gd_{82}$ core. On either side of the N = 82 shell closure, the moments indicate increasing collective effects. The onset of strong static ground state deformation between N = 88 and 89 is visible.

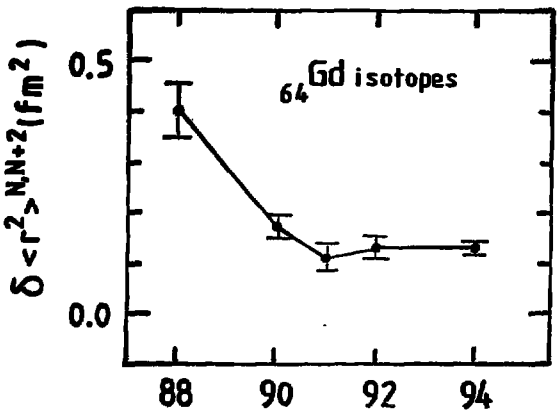

Figure XXIV : Isotope Shifts $\delta < r^2 >$ for Pairs of Gadolinium Nuclei ($_{83}$La).
The sudden fall of $\delta < r^2 >$ between 88 and 90 indicates the onset of deformation at N = 90.
Collective state character of deformed nuclei is observed for $90 \leq N \leq 94$, where $\delta < r^2 >$ is almost constant.

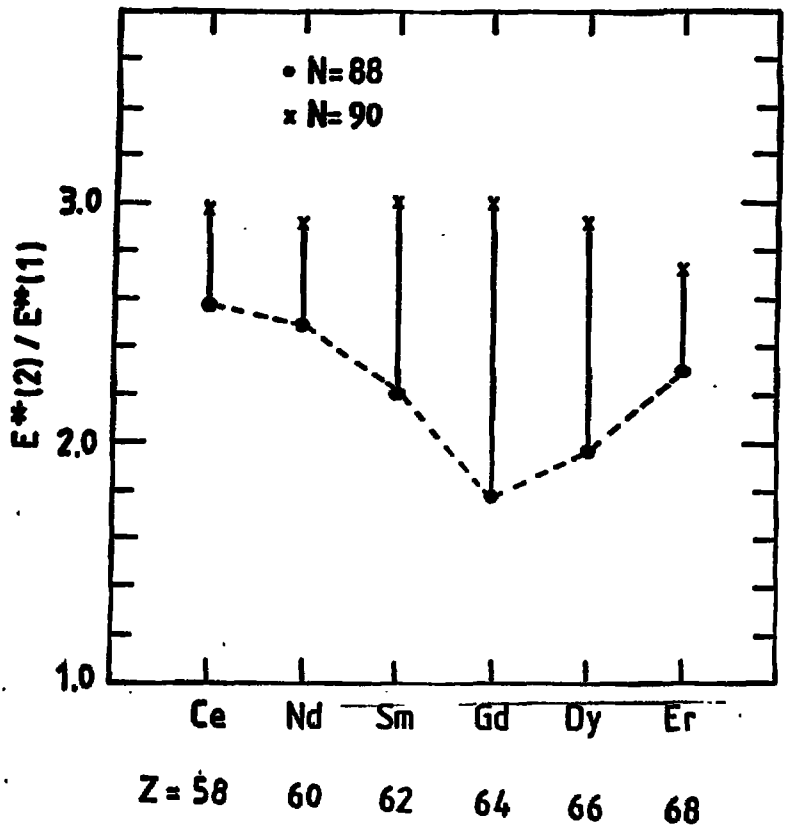

Figure XXV : Ratio $E^*(2)/E^*(1)$ of the Isotones $58 \leq Z \leq 68$ for N = 88 and 90 (see ref.9 in Introduction). $E^*(2)$ and $E^*(1)$ are the energies of the second and first excited levels of the nuclei. The lowest ratio for Gd for N = 88 and increasing deformations on either side of Z = 64 are signs of a probable subshell closure at this proton number. For N = 90, the ratio is almost constant.

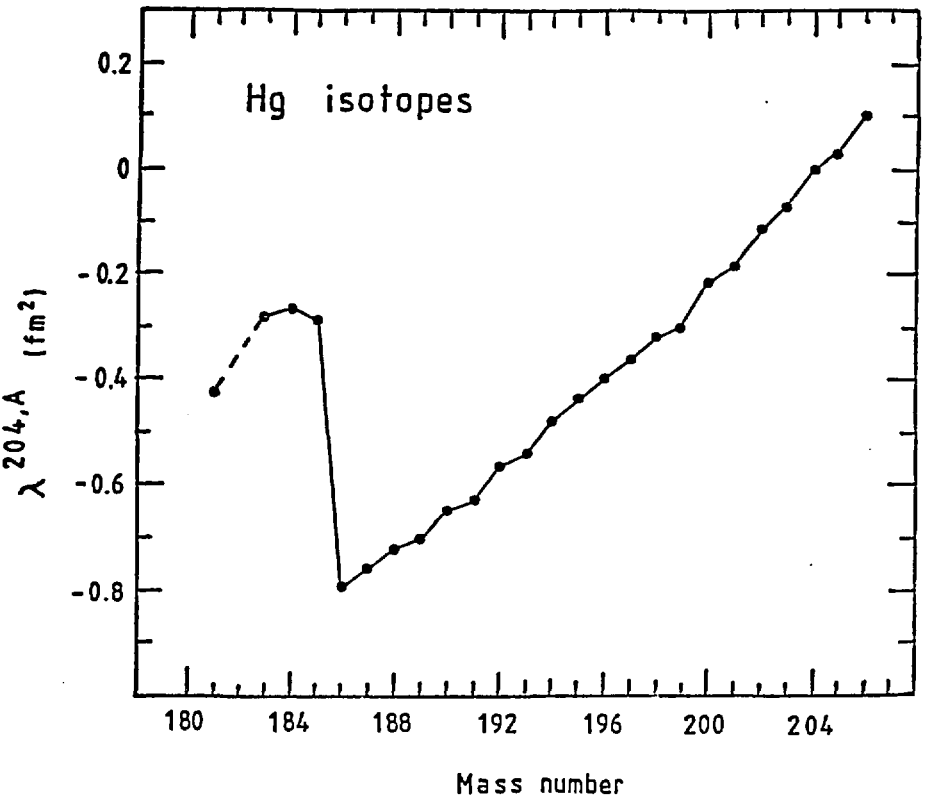

Figure XXVI : Parameter λ of Hg Isotopes Relative to ^{204}Hg (76Bo). $\lambda_{exp} = \delta \langle r^2 \rangle - 1.1 \times 10^{-3} \delta \langle r^4 \rangle + \ldots$ The series ^{205}Hg to ^{187}Hg shows a fairly regular decrease in charge radius. On reaching N = 105 i.e., near the middle of the neutron shell, the charge radius of ^{185}Hg jumps suddenly to that of ^{196}Hg(N = 116) having 10 % more neutrons. ^{183}Hg and ^{185}Hg have almost the same place. For ^{181}Hg, the slope of IS is back to normal. The observed jump in the Hg IS has been interpreted as a shape transition from a small oblate deformation in ^{187}Hg to a strong prolate one in ^{185}Hg.

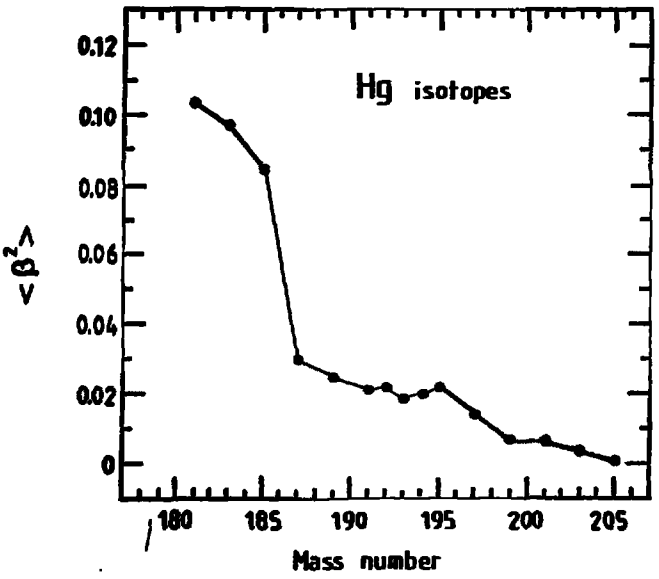

Figure XXVII : Squared Deformation Parameters for Hg Isotopes (76Bo). The value $\delta < \beta^2 > = 0.054(5)$ between mass numbers 186 and 187 indicates shape transition from a small oblate deformation in ^{187}Hg to a strong prolate one in ^{186}Hg.

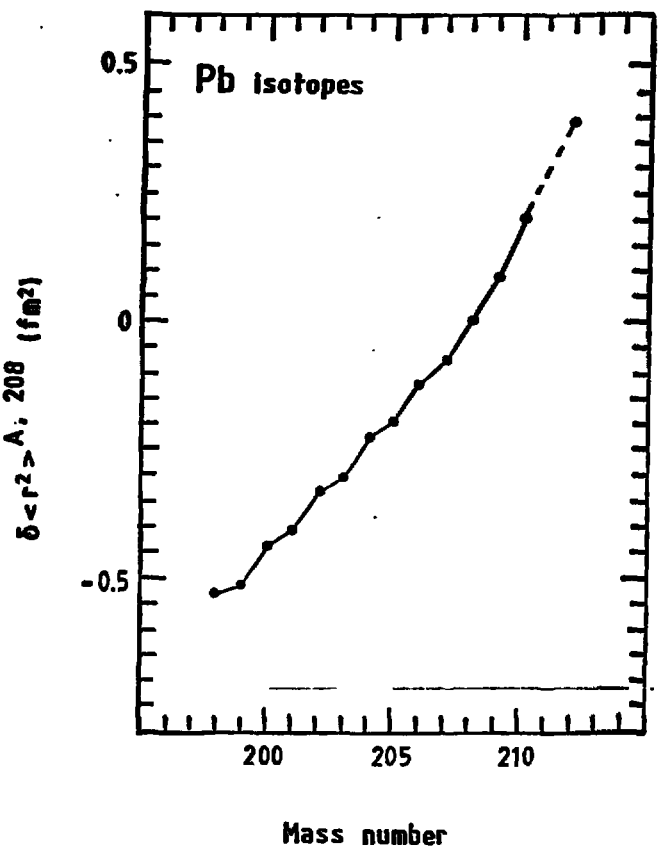

Figure XXVIII : $\delta \langle r^2 \rangle^{A,208}$ versus Mass Number of Pb Isotopes (83Th). There is a significant odd-even staggering in the variation of charge radii. $\delta \langle r^2 \rangle$ ch increases more rapidly when the neutrons start filling a new shell than when the shell is closed.

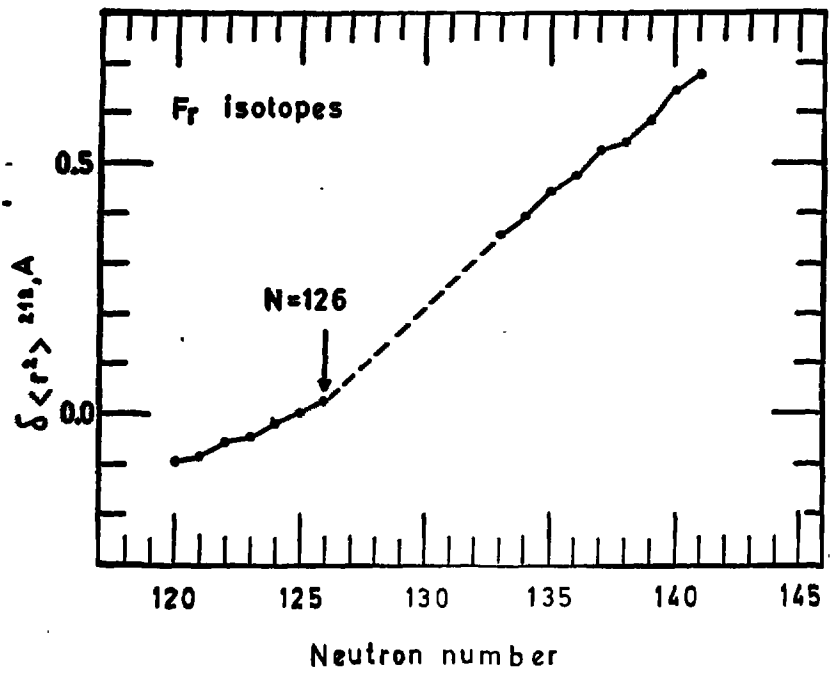

Figure XXIX : $\delta \langle r^2 \rangle^{212,A}$ vs Neutron Number for Fr Isotopes (85Co). A change in the mean slope at neutron shell closure at N = 126 is observed. The odd-even staggering is inverted for the N = 135 - 138 ($^{222-225}$Fr) and becomes again "normal" for N > 138.

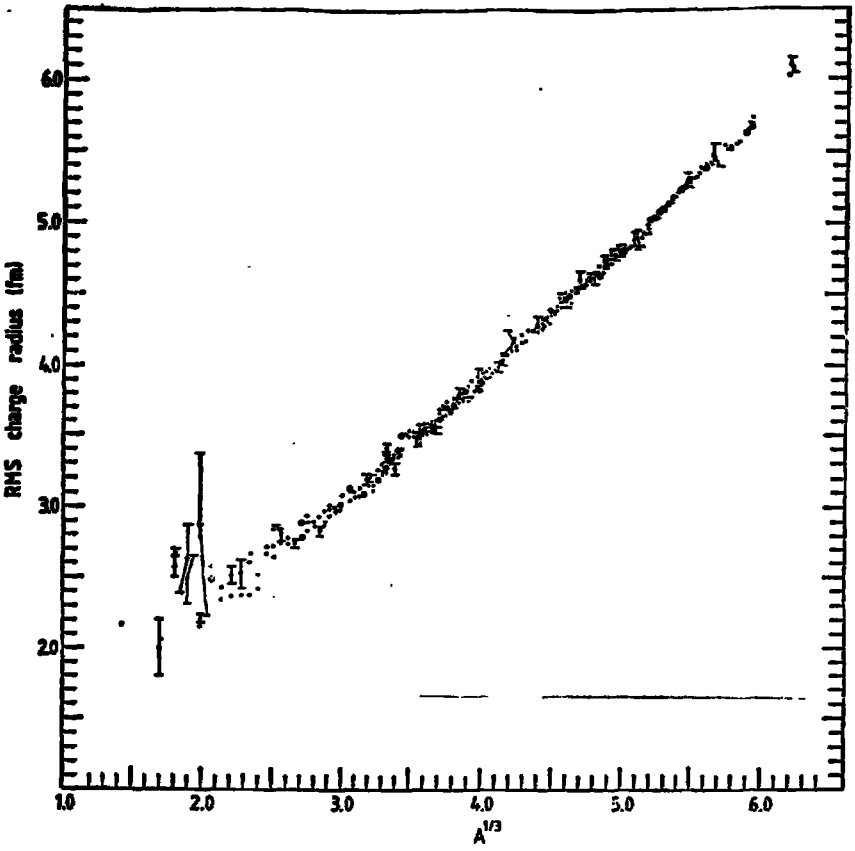

Figure XXX : Variations of RMS charge radius as with $A^{1/3}$ (86An). The $\langle r^2 \rangle^{1/2}$ values were deduced from experimental Coulomb displacement energies. The equation $\langle r^2 \rangle^{1/2} = 0.899\ A^{1/3} + 0.315$ is obtained from a least square fit analysis of data points.

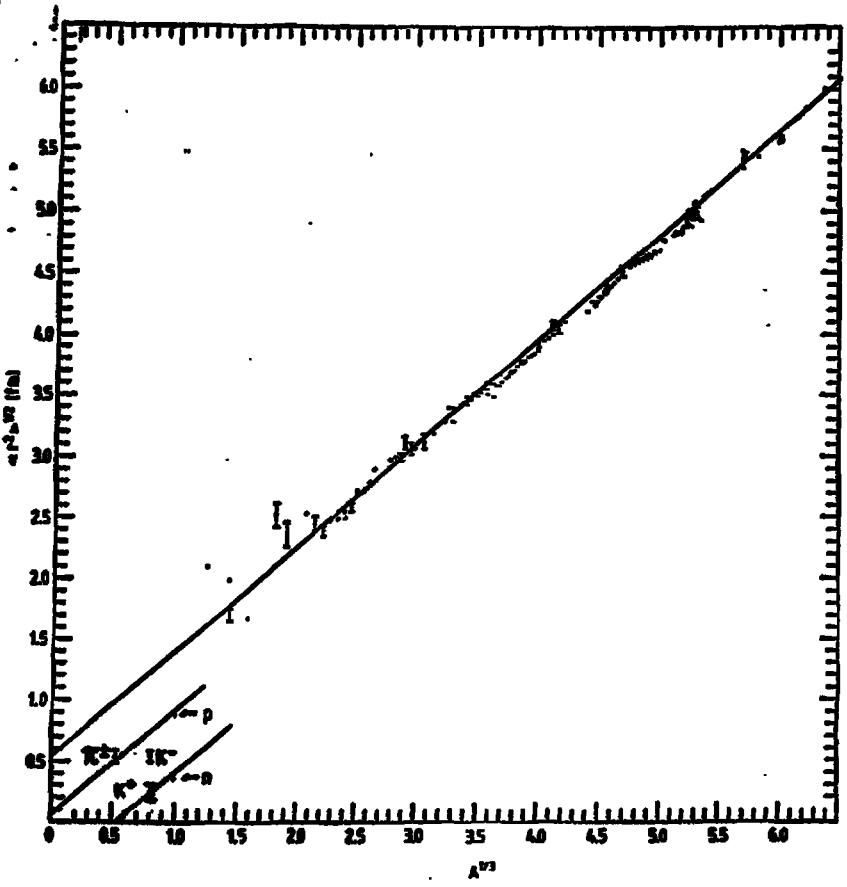

Figure XXXI : Experimental $< r^2 >^{1/2} = 0.857A^{1/3} + 0.465$ is obtained from a least squares fit analysis(86An).

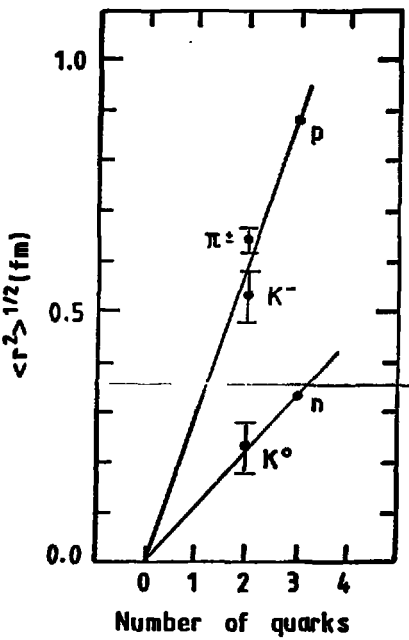

Figure XXXII : Experimental Root Mean Square Charge Radius as a Function of Number of Quarks. The RMS of a quark is deduced to be 0.3 fm from the straight line joining charged particles (86An).

References for TABLES I, II and III.

71Fa L.A.Fajardo, J.R.Ficenec, W.P.Trower, and I.Sick, Phys.Lett.37B, 363 (1971).

71He J.H.Heisenberg, J.C.McCarthy, I.Sick, and M.R.Yearian, Nucl.Phys.A164, 340 (1971).

72Bu F.A.Bumiller, F.R.Buskirk, J.N.Dyer and W.A.Monson, Phys.Rev.C5, 391(1972)

72Fi J.R.Ficenec, L.A.Fajardo, W.P.Trower, and I.Sick, Phys.Lett.42B, 213 (1972)

74Ch R.J.Champeau, J.J.Michel and H.Walther, J.Phys.B : Atom.Molec.Phys.7, L262 (1974).

74Da H.Daniel, H.-J.Pfeifer, K.Springer, P. Stoeckel, C.Backenstoss and L.Tauscher, Phys.Lett.48B,109 (1974).

74En R.Engfer, H.Schneuwly, J.L.Vuilleumier, H.K.Walter, and A.Zehnder, At.Data and Nucl.Data Tables 14, 509 (1974).

74Ja C.W.de Jager, H.de Vries, and C.de Vries, At.Data and Nucl.Data Tables 14, 479 (1974)

74Li G.C.Li, M.R.Yearian, and I.Sick, Phys. Rev.C9, 1861 (1974).

75Fi W.Fischer, H.Hühnermann, and Th.Meier, Z.Phys.A274, 79 (1975).

75Fu T.Fujita and A.Arima, Nucl.Phys.A254, 513(1975).

75Kl F.J.Kline, I.P.Auer, J.C.Bergstrom and H.S.Caplan, Nucl.Phys.A255, 435 (1975).

75Wo Wolfgang Shütz, Z.Phys.A273, 69 (1975).

76Bo J.Bonn, G.Huber, H.J.-Kluge, and E.W. Otten, Z.Phys.A276, 203 (1976).

76Ch H.Chandra and G.Sauer, Phys.Rev.C13, 245 (1976).

76Li J.W.Lightbody, Jr., S.Penner, S.P. Fivozinsky, P.L.Hallowell, and H. Crannell, Phys.Rev.C14, 952 (1976).

76Ro H.Rothhaus, Ph.D Thesis, Universität Mainz (1976).

76Sh E.B.Shera, E.T.Ritter, R.B.Perkins, G.A.Rinker, L.K.Wagner, H.D.Wohlfahrt, G.Fricke, and R.M.Steffen, Phys.Rev. C14, 731 (1976).

77Ba R.C.Barrett and D.F.Jackson, and references therein in *Nuclear Sizes and Structure*,(Clarendon Press, Oxford, (1977) p.142.

78Au P.Aufmuth, H.-P.Clieves, K.Heilig, A. Steudel, D.Wendlandt, and J.Bauche, Z.Phys.A285, 357 (1978)

78Hu G.Huber, F.Touchard, S.Büttgenbach, C.Thibault, R.Klapisch, H.T.Duong, S.Liberman, J.Pinard, J.L.Vialle, P.Juncar, and P.Jacquinot, Phys.Rev. C18, 2342 (1978)

78Kl J.C.Kim, R.S.Hicks, R.Yen, I.P.Auer, H.S.Caplan, and J.Bergstrom, Nucl.Phys. A297, 301 (1978)

78Sc L.A.Schaller, T.Dubler, K.Kaeser, G.A. Rinker, Jr., B.Robert-Tissot, L. Schellenberg, and H.Schneuwly, Nucl. Phys.A300, 225 (1978)

79Be A.Bekk, A.Andl, S.Göring, A.Hanser, G.Howicki, H.Rebel, and G.Schatz, Z. Physik A291, 219 (1979)

79Cl D.L.Clark, H.E.Cage, D.A.Lewis and G.N. Greenless, Phys.Rev.A20, 239 (1979).

79Da P.Dabkiewicz, F.Buchinger, H.Fischer, H.-J.Kluge, H.Kremmling, T.Kühl, A.C. Mütler and H.A.Schnessler, Phys.Lett. B82, 199 (1979)

79Ge H.Gerhardt,E.Matthias, H.Rinneberg, F.Schneider,A.Timmermann, R.Wenz, and P.J.West,Z.Physik. A292, 7 (1979)

79Ko J.Kowalski, F.Träger, S.Weisshaar, H.-B.Wiegemann, and G.zu Pulitz, Z.Phys. A290, 345 (1979)

80Br1 H.Brand, B.Seibert, A.Steudel, Z Physik.A296, 281 (1980)

80Br2 W.J.Briscoe, H.Crannell and J.C. Bergstrom, Nucl.Phys.A344, 475 (1980)

80Ca J.H.Cavedon, Ph.D.Thesis, Orsay (1980)

80Sc L.Schellenberg, B.Robert-Tissot, K. Käser, L.A.Schaller, H.Schneuwly, G. Fricke, S.Glückert, G.Mallot, and E.B. Shera, Nucl.Phys.A333, 333 (1980)

80St A.Steudel, U.Triebe, and D.Wendlandt, Z.Phys.A296, 189 (1980)

81Bä A.Bäcklin, N.G.Jonsson, R.Julin, J.Kantele, M.Luontama, A.Passoja and T.Poikolainen, Nucl.Phys.A351, 490 (1981)

81Ho M.V.Hoehn, E.B.Shera, H.D.Wohlfahrt, H.Yamazaki, R.M.Steffen, and R.K. Sheline, Phys.Rev.C24, 1667 (1981).

81Mo H.A.Moinester, J.Alster, G.Azuelos, J.B.Bellicard, B.Frois, M.Huet, P. Leconte, and Phan Xuan Ho, Phys.Rev. C24, 80 (1981).

81Ol A.Olin, P.R.Poffenberger, G.A.Beer, J.A.Macdonald, G.R.Mason, R.M.Pearce and W.C.Sperry, Nucl.Phys.A360, 426 (1981).

81Th1 C.Thibault, F.Touchard, S.Büttenbach, R.Klapisch, M.de Saint Simon, H.T. Duong, P.Jacquinot, P.Juncar, S. Liberman, P.Pillet, J.Pinard, J.L. Vialle, A.Pesnelle and G.Huber, Phys.Rev.C23, 2720 (1981)

81Th2 C.Thibault, F.Touchard, S.Büttenbach, R.Klapisch, M.de Saint Simon, H.T. Duong, P .Jacquinot, P.Juncar, S. Liberman, P.Pillet, J.Pinard, J.L. Vialle, A.Pesnelle, The Isolde Collaboration, and G.Huber, Nucl.Phys.A367, 1(1981).

81We R.Wenz, A.Timmermann and E.Matthias, Z.Phys.A303, 87 (1981).

81Wo H.D.Wohlfahrt, E.B.Shera, M.V.Hoehn, Y.Yamazaki, and R.M.Steffen, Phys.ReV. C23, 533 (1981).

82An A.Andl, K.Bekk, S.Göring, A.Hanser, G.Nowicki, H.Rebel, G.Schatz, and R.C. Thompson, Phys.Rev.C26, 2194 (1982)

82Bu F.Buchinger, A.C.Mueller, B.Schinzler, K.Wendt, C.Ekström, H.Klempt, R.Neugart and the ISOLDE Collaboration, Nucl.Instr. and Meth.202, 159 (1982).

82Sc L.A.Schaller, L.Schellenberg, T.Q.Phan, G.Piller, A.Ruetschi, and H.Schneuwly, Nucl.Phys.A379, 523 (1982).

82Sh E.B.Shera, H.D.Wohlfahrt, M.V.Hoehn, and Y.Tanaka, Phys.Lett.112B, 124 (1982).

82To F.Touchard, P.Guimbal, S.Büttenbach, R.Klapisch, M.de Saint Simon, J.M. Serre, C.Thibault,H.T.Huong, P.Juncar, S.Liberman, J.Pinard and J.L.Vialle, Phys.Lett.108B, 169 (1982)

83Ah S.A.Ahmad, W.Klempt, R.Neugart, E.W. Otten, K.Wendt, C.Ekström and the ISOLDE Collaboration, Phys.Lett.133B, 47 (1983).

83Ba P.E.G.Baird, S.A.Blundell, G.Burrows, C.J.Foot, G.Meisel, D.N.Stacey and G.K.Woodgate, J.Phys.B : At.Mol.Phys. 16, 2485 (1983).

83Kl H.J.Kluge, H.Kremling, H.A. Schuessler, J.Streib, and E.Wallmeroth, Z.Phys.A309, 187 (1983).

83Ku W.Kurcewicz, N.Schneider, L.H.Simons, J.Nust and R.Abela, Z.Phys.A312, 11 (1983).

83Le D.D.Leabacher, Y.Tanaka, R.M.Steffen, E.B.Shera, and M.V.Hoehn, Phys.Rev. C27, 1772 (1983).

83Mu A.C.Mueller, F.Buchinger, W.Klempt, E.W.Otten, R.Neugart, C.Ekström, J. Heinemeier, and the Isolde Collaboration, Nucl.Phys.A403, 234 (1983).

83Ry D.Rychal, H.J.Emrich, H.Miska, R. Gyufko, and C.A.Wiedner, Phys.Lett. 130B, 8 (1983).

83Th R.C.Thompson, H.Anselment, H.Bekk, S. Göring, A.Hanser, G.Meisel, H.Rebel, G.Schatz, and B.A.Brown, J.Phys.G : Nucl.Phys.9, 443 (1983).

84Be D.Bender, N.Brand and Y.Pfeufer, Z.Phys.A318, 291 (1984).

85Ah S.A.Ahmad, W.Klempt, C.Ekström, R. Neugart, and K.Wendt, Z.Phys.A321, 35 (1985).

85Be A.Bernard, H.Brüggemeyer and Y.Pfeufer, Z.Phys.A322, 1 (1985).

85Bo F.W.N. de Boer, B.Ass, P.Baertschi, W.Beer, I.Beltrami, K.Bos, P.F.A. Goudsmit, D.Kiebele, B.Jeckelmann, H.J.Leisi, W.Ruckstuhl, G.Strassner, A.Vacchi, and R.Weber, Nucl.Phys.A444, 589 (1985).

85Co A.Coc, C.Thibault, F.Touchard, H.T. Duong, P.Juncar, S.Liberman, J.Pinard, J.Lerme, J.L.Vialle, S.Büttgenbach, A. C.Mueller, A.Pesnelle and the ISOLDE Collaboration, Phys.Lett.163B, 66 (1985)

85Ot C.H.Otterauer, C.Ribbschall, R.Neurer, R.Ehrlich, Ch.Schmitt and V.H.Walther, Nucl.Phys.A436, 688 (1985).

85St J.Streib, H.-J.Kluge, H.Kremling, R.B. Moore, H.W.Schaaf, and E.Wallermath, Z.Phys.A321, 537 (1985).

85Ul G.Ulm, Scientific Report GSI-85-1, March 1985, p.79.

86An M.S.Antony, Thesis, Docteur ès-Sciences, Université de Strasbourg, July 1986.

Additional Data

Element	A	μ_n(n.m)	Method	Reference
I	117	3.1 (2)	OLLTNO	86Gr
	118	2.0 (2)	OLLTNO	86Gr
	118m	4.2 (2)	OLLTNO	86Gr
	119	2.9 (1)	OLLTNO	86Gr
	120	1.23 (3)	OLLTNO	86Gr
	120m	4.2 (2)	OLLTNO	86Gr
	121	2.3 (1)	OLLTNO	86Gr
	122	0.94 (3)	OLLTNO	86Gr

Comment : The μ_n values measured by the technique of On-Line Low-Temperature Nuclear Orientation illustrate the influence of

(1) spherical and deformed β-decaying states in the same nucleus

and

(2) the N = 64 subshell gap (86Gr).

The ground state moments show the influence of N = 64 subshell closure with near spherical configurations, whereas the moments of metastable states suggest large prolate deformations.

86 Gr V.R.Green, N.J.Stone, T.L.Shaw, J.Rikovska, K.S.Krane, P.M.Walker and I.S.Grant, Phys.Lett. 173B, 115 (1986).

Imprimé
au Centre de
Recherches Nucléaires
Strasbourg
1986